EVALUATION OF SWITCH-MODE POWER SUPPLIES IN A MAGNETOENCEPHALOGRAPHY SYSTEM

Lappeenranta–Lahti University of Technology LUT

Master’s Programme in Electrical Engineering, Master's thesis

2023

Lasse Holopainen

Examiner(s): Professor, Pertti Silventoinen

Petteri Laine, Megin Oy

ABSTRACT

Lappeenranta–Lahti University of Technology LUT

LUT School of Energy Systems

Electrical Engineering

Lasse Holopainen

Evaluation of Switch-Mode Power Supplies in a Magnetoencephalography System

Master's thesis

2023

46 pages, 31 figures, 3 tables and 2 appendices

Examiners: Professor Pertti Silventoinen and Petteri Laine, Megin Oy

Keywords: DC-DC power converters, Switch-Mode power supply, Power quality, Electromagnetic interference, Biomedical electronics

The Megin Triux Neo, an MEG system, is a biomedical diagnostic and research instrument for locating and timing bioelectric activity inside the brain. It uses superconducting sensors, submerged in liquid helium to measure the magnetic field changes outside the subject's head, caused by the brain's neuronal electric currents.

This study investigates the feasibility of replacing the original linear power supplies of the MEG system with switch-mode power supplies. The MEG system, measuring the weak femtotesla-level magnetic fields, is also sensitive for electromagnetic disturbances, so the switching related noise in the measurement data needs to be examined carefully.

A prototype switch-mode power supply unit is assembled with commercially available SMPS modules, inside the existing linear power supply unit enclosure, with original connectors, to fit the prototype unit in place of the existing one in the system.

Both the original and the prototype power supplies are tested to compare the nominal characteristics, and to distinguish power supply originated from the other sources of noise. The power supplies are first bench tested with resistive loads, then presentable active loads, and finally with empty-room MEG measurements with a fully functional system.

The tests with the SMPS unit did not reveal any obvious performance degradation. The overall noise in the MEG measurement remained at the same level. The tests were limited to the digital electronics of the system and should be extended to the analog front end before the switch-mode power supplies can be ultimately determined feasible in this application.

TIIVISTELMÄ

Lappeenrannan–Lahden teknillinen yliopisto LUT

LUT Energiajärjestelmät

Sähkötekniikka

Lasse Holopainen

Hakkuritehonlähteiden soveltuvuuden arviointi magnetoenkefalografiajärjestelmässä

Sähkötekniikan diplomityö

2023

46 sivua, 31 kuvaa, 3 taulukkoa ja 2 liitettä

Tarkastaja(t): Professori Pertti Silventoinen ja Petteri Laine, Megin Oy

Avainsanat: DC-DC tehonmuuntimet, hakkuritehonlähteet, tehon laatu, sähkömagneettiset häiriöt, lääketieteellinen elektroniikka

Megin Triux neo, MEG-järjestelmä, on biolääketieteellinen mittausjärjestelmä, joka hyödyntää nestemäiseen heliumiin upotettuja suprajohtavia sensoreita aivojen sähköisen toiminnan mittaamiseen pään ulkopuolelta. Järjestelmää käytetään lääketieteen diagnostiikassa sekä perustieteellisessä tutkimuksessa.

Tässä diplomityössä tutkitaan mahdollisuutta korvata järjestelmän käyttämiä lineaarisia tehonlähteitä hakkuritehonlähteillä. MEG-järjestelmä, joka mittaa hyvin heikkoja femtotesla-tasoisia magneettikenttiä, on herkkä myös sähkömagneettisille häiriöille, joten mahdolliset hakkureiden aiheuttamat häiriöt mittausdatassa on tutkittava huolellisesti.

Hakkuritehonlähteitä arvioidaan kokoamalla kaupallisesti saatavilla olevista hakkurimoduuleista koekappale, joka hyödyntää olemassa olevan tehonlähteen koteloa ja liittimiä, jotta sitä voidaan testata järjestelmässä olemassa olevan tehonlähteen tilalla.

Sekä olemassa olevan että koekappaleen jännitelähtöjen laatua arvioidaan, jotta voidaan erottaa tehonlähteestä aiheutuvat häiriöt ulkoisista häiriöistä. Tehonlähteitä arvioidaan ensin vastuskuormalla, jonka jälkeen käytetään todenmukaista aktiivista kuormaa, ja lopuksi tehdään tyhjän huoneen MEG-kohinamittauksia kokonaisella järjestelmällä.

Tehonlähteiden arvioinnissa ei tullut esiin merkittävää laadun heikentymistä. Häiriöiden kokonaisarvio MEG-mittauksissa pysyi samalla tasolla. Arviointi rajoittui digitaaliseen tiedonkeruuelektroniikkaan ja arviointi tulisi laajentaa myös analogiseen etuasteeseen, jotta voidaan päästä varmuuteen siitä, soveltuvatko hakkuritehonlähteet tähän käyttökohteeseen.

ABBREVIATIONS

LSB	Least significant bit
LED	Light emitting diode
FFT	Fast Fourier transform
MEG	Magnetoencephalography
DC	Direct current
AC	Alternating current
EMI	Electromagnetic interference
SMPS	Switch-mode power supply
EMC	Electromagnetic compatibility
MSI	Magnetic source imaging
MRI	Magnetic resonance imaging
SQUID	Super conducting quantum interference device
MSR	Magnetically shielded room
OPM	Optically pumped magnetometer
LDO	Low-dropout (regulator)
PWM	Pulse width modulation
MDR	Medical device regulation
IVD	In-vitro diagnostics
EEG	Electroencephalography
PSU	Power supply unit
PCB	Printed circuit board

Table of contents

1 Introduction

This study for Megin Oy aims to analyse the feasibility and possible adverse effects of using switch-mode power supplies in their product, Triux neo MEG-system. Due to the system being designed to record extremely weak magnetic fields emanating from the living human brain, it's also sensitive to surrounding electromagnetic disturbances. The main electronics of the system are currently powered with linear power supplies for their known low noise DC-output voltage and low EMI. The motivation to evaluate the switch-mode technology is its ability to perform significantly more efficiently, reducing wasted energy, need for excess heat removal, size, weight, and cost, which makes it attractive alternative for powering the electronics. The SMPS' generate high frequency switching noise that may make its way into the MEG-measurement data, reducing the signal quality over a wide frequency band, which is the main concern of this study. The wideband RF-reception and nonlinearity of the sensor elements cause challenges with RF-interference mixing to the signal of interest.

The effects of the SMPS are examined by assembling a prototype switch-mode power supply unit and testing it against the original specifications and head-to-head with the original linear power supply with passive and active loads and finally in the actual operational MEG-system for signal quality analysis. The system-EMC is ruled out of the scope of this study, but it is a necessary consideration in possible further evaluation of the technology.

The results of this study may be used as a pretext for further investigation for SMPS application and as supporting notes for future product development decision making.

Following subsections introduce the background of the MEG, switch-mode power supplies, linear power supplies and relevant electrical safety aspects in medical device regulation.

1.1 About the MEG

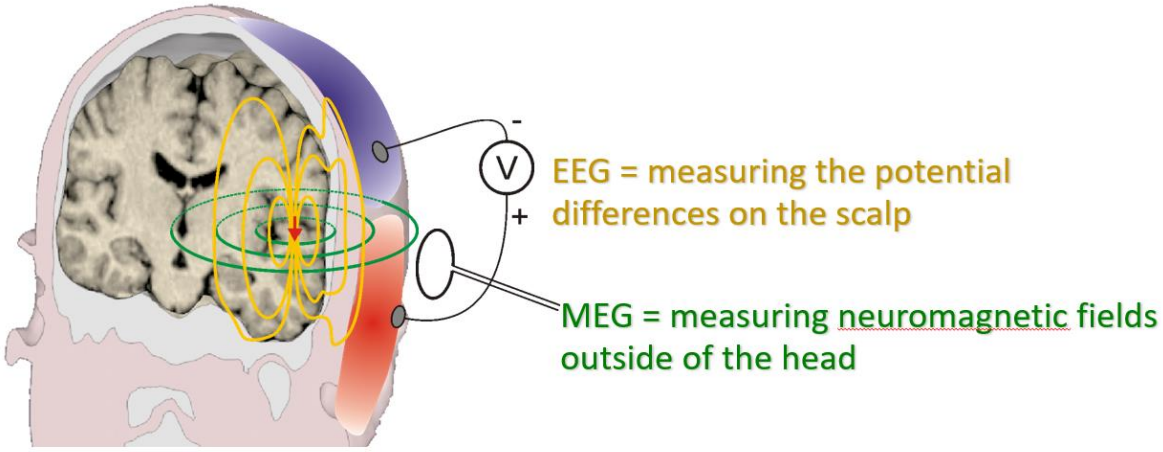

Figure 1. Principle of MEG and EEG. (Megin Customer Training Material)

Magnetoencephalography is a biomedical measurement method for recording the electromagnetic activity of the brain. The weak magnetic fields outside the skull, caused by the bioelectric neural signalling, are recorded with sensitive magnetometers located closely around the subject's head (Hämäläinen et al., 1993). Figure 1 shows the close relation to electroencephalography, EEG. The origin of the measured physical quantities is the same, the neural bioelectricity, which in EEG, is interpreted from the potential differences of the scalp, and in MEG, external magnetic field fluctuations. Figure 2 illustrates the signal acquisition of the whole-head MEG-sensor array.

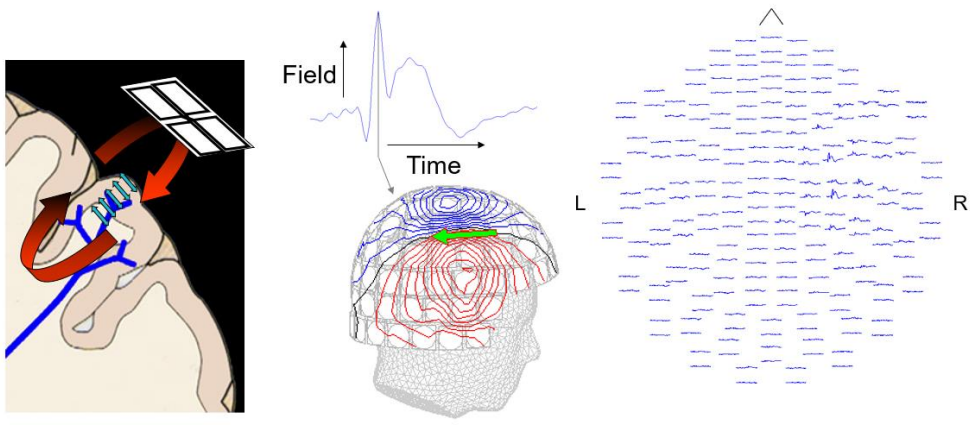

Figure 2. MEG Signals. (Megin Customer Training Material)

In conjunction with clever mathematical modelling and knowledge of the signal source, the recorded neural activity can be located in few millimetres' accuracy in a procedure of Magnetic Source Imaging, MSI, and superimposed on a structural MRI-image as illustrated at the right side of figure 3. The MEG has many potential and established research and clinical applications, where precise locating and timing of the brain function are important (Maldjian et al. 2022).

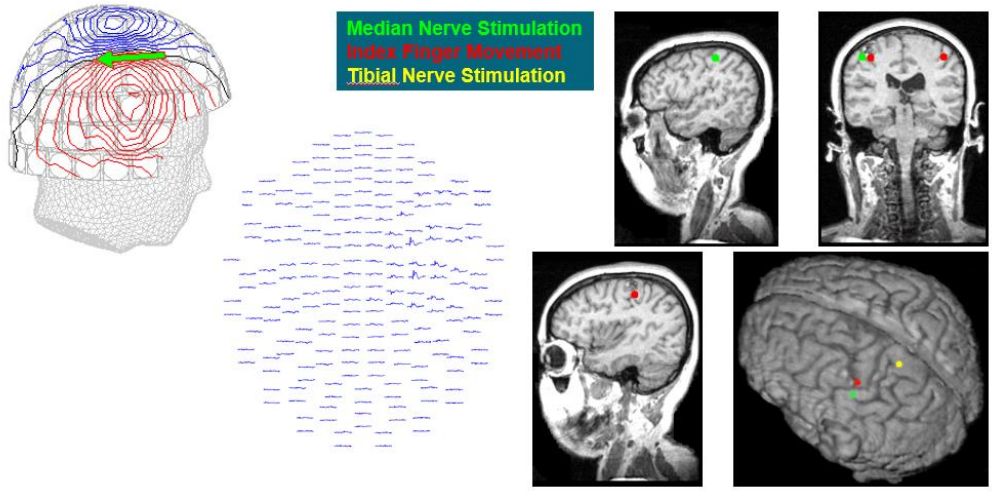

Figure 3. Magnetic Source Imaging. (Megin Customer Training Material)

The history of the MEG goes back to late 1960's and early 1970's when the first MEG measurements were made in the United States by David Cohen from the University of Illinois. The first measurements were made with a copper coil detector, before introduction of the Super Conducting Quantum Interference Device, SQUID, by James Zimmerman from Ford Motor Company. The first SQUID-based MEG-measurement were conducted again by David Cohen in Massachusetts Institute of Technology, MIT in 1971. The SQUID requires cooling down with liquid helium to super conducting state at around 4 K temperature to

operate. Figure 4 is a photograph of Dr Cohen’s megnetically shielded room. (Cohen, 1968) (Zimmerman, Thiene and Harding 1970) (Cohen, 1972)

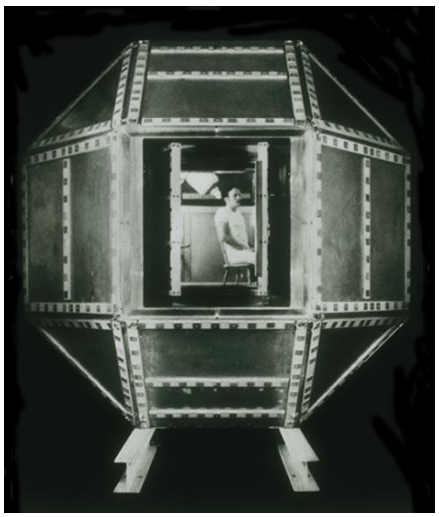

Figure 4. Dr. Cohen's shielded room at MIT (David Cohen)

In Finland, the research on biomagnetism and SQUIDs continued in Helsinki University of Technology Low Temperature Laboratory led by Olli Lounasmaa in the 1970’s. In 1980, brain research was chosen as a field of research for the laboratory and their first one-channel MEG-device was put into service soon thereafter (Fig. 5).

Figure 5. One channel MEG in early 1980's. (Low Temperature Laboratory, Aalto University archives)

In 1989, a spin-off company Neuromag Oy (nowadays Megin Oy) was founded to commercialize the ongoing MEG-technology research. The Finnish Innovation Fund, SITRA, already significantly funding the research, became the majority shareholder and Mustekala Ky (squid, the animal, in Finnish), a limited partnership company of six research team members committed to a minority share. The first whole-head MEG system with 122 channels was inaugurated in 1992, and in 1998 followed the 306-channel system, which are direct ancestors of the present-day Megin product. (Megin Oy archives, 1989) (Heikkilä, 2014)

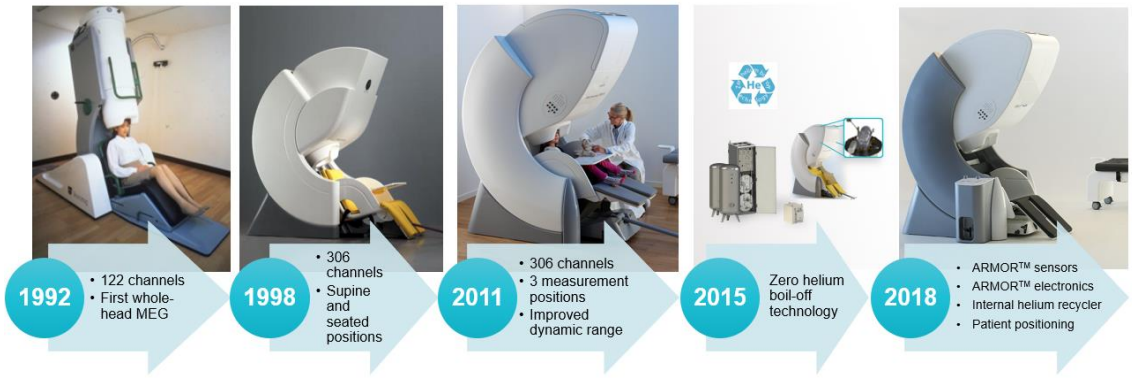

Figure 6. History of MEGIN instrumentation. (Megin Customer Training Material)

The current Megin Triux neo system is equipped with state-of-the-art SQUID sensors (Fig. 7), simultaneous EEG recording and other practical improvements around the core MEG-system such as the internal helium recycling and software utilities for data acquisition, analysis and visualization.

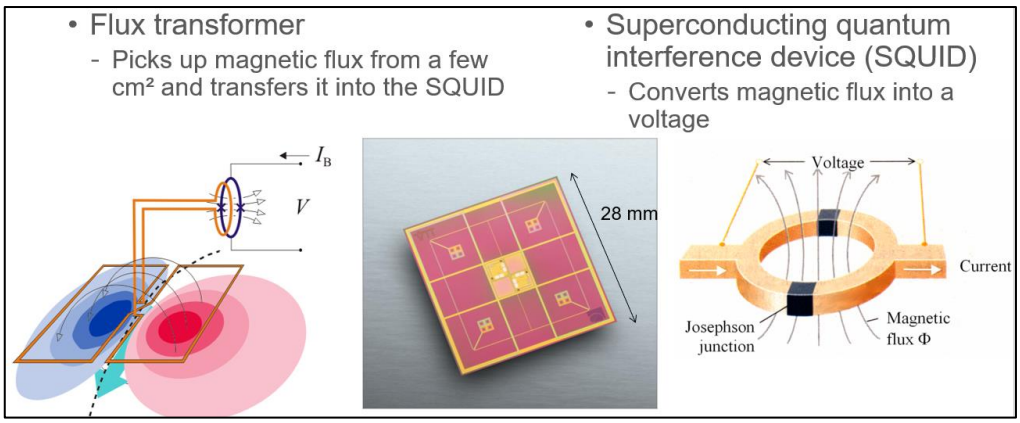

Figure 7. ARMOR™ sensor. (Megin Customer Training Material)

The main system parts are located inside and outside of a magnetically shielded room, the MSR. Inside the MSR is the probe unit with the SQUID sensors submerged in liquid helium, pre-amplifiers and control electronics, and the patient bed/chair. The MSR shields the sensitive measurement equipment from the environmental magnetic activity which is generally many orders of magnitude higher than the measured brain signals. Outside the MSR are located the filter cabinet, the main electronics cabinet, and the stimulus cabinet. The filter cabinet acts as an electrical interface between the MSR and the outer world and provides heavy filtering for all signals going in and out of the MSR. The main electronics cabinet holds the data acquisition and control electronics as well as an array of linear power supplies which provide power to the core electronics. The stimulus cabinet holds an application specific selection of equipment providing different types of sensory stimuli to the patient for evoked response studies. Also, outside the MSR resides a direct-online single-phase AC-motor that tilts the probe unit to different positions. Figure 8 shows the main system parts.

Figure 8. Internal Helium Recycler. (Megin Customer Training Material) Image also shows conveniently most of the main system parts. The probe unit [A], the MSR [B], the filter cabinet [C], the main electronics cabinet [D], the stimulus cabinet [E], the lifting motor [F].

The latest research activity around MEG sensor technology in the past few years has been the utilization of the Optically Pumped Magnetometer, OPM. Instead of superconducting sensors, that require near absolute zero temperature to operate, OPMs rely on the nuclear

magnetic resonance phenomenon - theory related also to the MRI. In principle, an OPM consists of a laser, an alkali atom vapor chamber and a photodetector. The laser light is circularly polarized using a quarter-wave plate, after which it is passed through the vapor. The circularly polarized light brings the vapor to a magnetically sensitive state by creating a net spin-polarization ("optical pumping"). Changing external magnetic field affects the spin-polarization of the vapor in such a way that can be detected, as a function of the magnetic field, from the light passing through the vapor.

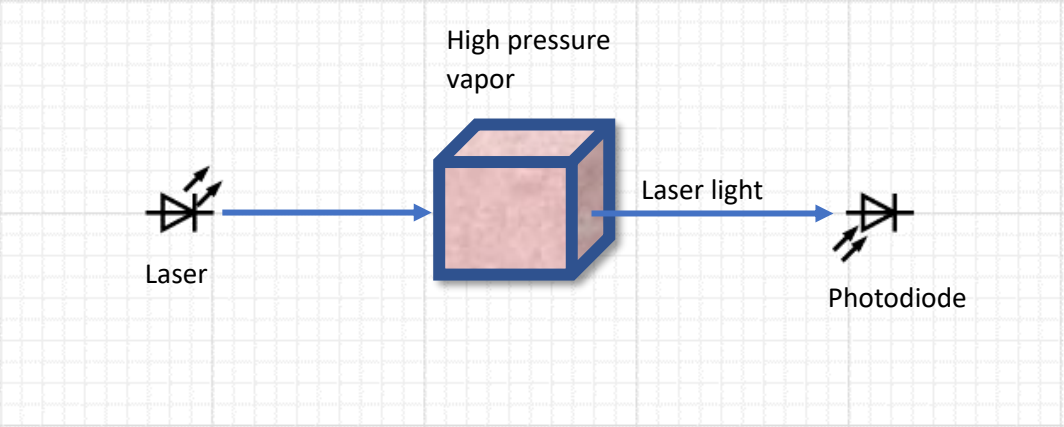

Figure 9. General OPM schematic presentation

The OPM is sometimes seen as a potential future alternative for the SQUID in the MEG. The advantages are freer placement of the sensors and closer proximity to the brain as the insulation between cryogenics and scalp is not required. The practical white noise level of the OPM is still much higher (10-100 fT/√Hz) than of the SQUID (~2 fT/√Hz). The OPM technology is currently being developed by many, more or less linked, research groups around the world. (Tierney et al., 2019)

1.2 The Linear and Switch-Mode Power Supplies

A linear AC to DC power supply in principle consists of a line-frequency transformer, a rectifier stage, and a transistor, that is used in its linear region as a variable resistor. The

mains level AC voltage is first lowered with the transformer, rectified with a diode bridge, and then regulated with the transistor. The efficiency of a linear power supply is in the range of 50 to 60 % at best and the remainder is turned to heat, which needs to be dissipated with heavy heat sinks and/or fans. The linear power supplies are considered nowadays heavy, bulky, and inefficient, and their use in mainstream electronics has practically ended. Figure 10 shows a schematic presentation of a linear power supply.

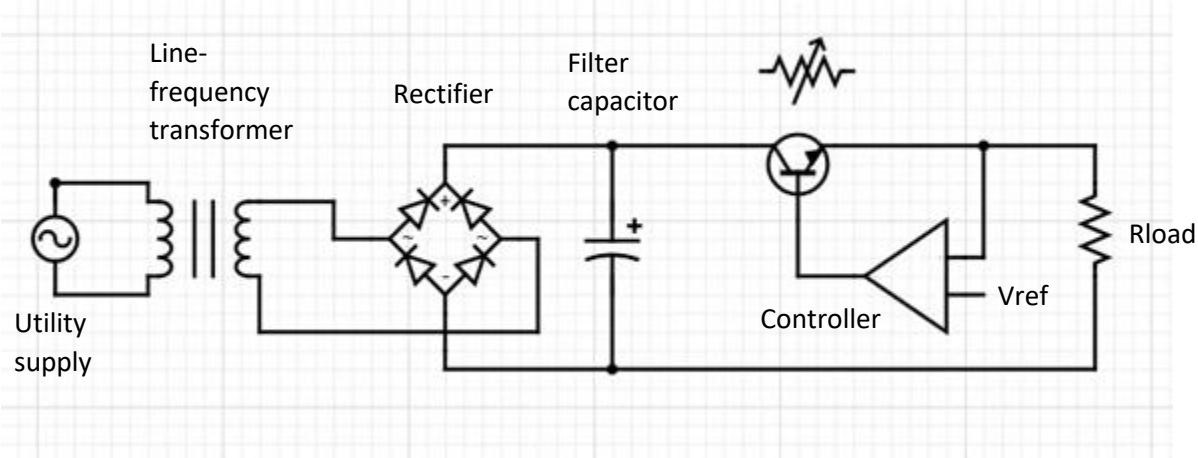

Figure 10. Linear dc power supply schematic presentation.

The galvanic isolation boundary between the mains AC input and power supply DC output, is at the line-frequency transformer. The main advantages of linear power supplies are simple and robust design, stable voltage regulation and low noise DC output.

Though the wide use of linear technology in AC to DC power supplies has diminished, the linear DC to DC regulators, known as low-dropout, LDO, regulators, are still widely used in point-of-load applications. As the main higher power regulators may be the switching type, there is often use for dedicated low power linear regulators for sensitive components, such as ADCs, DACs or multipurpose processor chips that require low noise supply. (Gunawardane et al., 2022)

The switch-mode power supply regulates the voltage also with a transistor, not as a variable resistor, but by switching rapidly fully on and off in a scheme generally known as pulse width modulation, PWM. The resulting square-wave is then rectified and filtered to stable DC. The other major difference is that the mains voltage does not have to be first lowered

with a massive line-frequency transformer, but it can be directly rectified before the switching transistor. Figure 11 shows a schematic presentation of a switch-mode power supply.

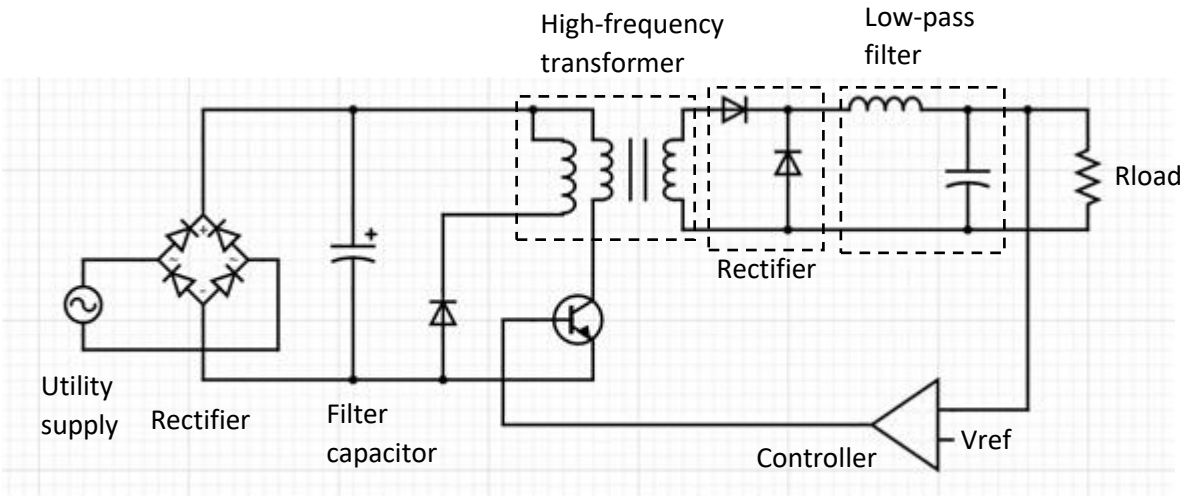

Figure 11: Switch-mode power supply schematic presentation.

The high frequency transformer after the switching stage provides an additional voltage step and an isolation boundary between mains network and the power supply output. (Mohan, Undeland and Robbins 2003)

The swich-mode power supplies can achieve 90% efficiency. There is still heat generated mainly in the on-state resistance and the turn-on and -off times of the semiconductors. The losses can be lowered by faster switching frequency and turn-on-off times, but it leads to higher frequency noise spectrum and difficult electromagnetic interference issues (Rashid, 2011). The SMPS' require filtering for both input and output for conducted interference and possibly shielding and advanced PCB techniques to counter radiated interference (Ott, 1988).

Numerous recent research articles involving SMPS' concentrate around the electromagnetic emissions. Either development and suggestion of novel topologies and control (Manjunath, Sudheer 2020) and (Subotskaya, Bodano and Deutschmann 2020) or modelling of the conducted and radiated emissions (Iqbal et al., 2020), (Bykhovsky, 2022) and (Leferink, Roc'h 2011).

1.3 Medical Device Electrical Safety Regulation

Medical device electrical safety regulation is an important area of regulatory compliance for medical devices. Medical devices that rely on electricity for their operation must meet certain safety requirements to ensure that they do not pose any risk to patients or operators.

In the European Union, medical device electrical safety is regulated by the Medical Device Regulation (MDR) and the In Vitro Diagnostic Regulation (IVDR). These regulations require medical device manufacturers to demonstrate compliance with relevant standards for electrical safety, including the International Electrotechnical Commission, IEC 60601 series of standards. (The European Parliament and the Council of The European Union, 2017)

In the United States, medical device electrical safety is regulated by the Food and Drug Administration, FDA, under the Federal Food, Drug, and Cosmetic Act, FD&C Act, and the Code of Federal Regulations, CFR. This regulation requires that medical devices be designed and manufactured in accordance with recognized engineering standards to ensure their electrical safety. The FDA also requires that medical device manufacturers provide documentation demonstrating compliance with applicable electrical safety standards. (U.S. Food & Drug Administration)

Other countries have their own regulations governing medical device electrical safety. For example, Health Canada regulates medical devices under the Medical Devices Regulations, which require compliance with the IEC 60601 series of standards. (Health Canada, 2023)

In practice, the patient and the device operator should be protected from dangerous currents flowing through their body parts in contact with the device, even in predictable fault scenarios. In careful risk assessment, some multi-step failure modes may be deemed so incredibly rare that, with all the mitigations in place, the associated risk is negligible.

The MEG recording doesn’t require the patient to touch the device as such, but the other essential features such as the EEG and head position indicator coils need to be directly attached to the patient making contact points to electrical devices.

The isolated power supply is one link in the chain of several means to protect the patient from dangerous body currents and this needs to be taken into account in the specification of the power supply. The relevant parameters are (capacitive) leakage currents from the mains supply, the dielectric strength of the insulations and sufficient creepage and clearance distances.

2 Methods

To evaluate the feasibility of utilizing Switch-mode power supplies in MEG system the chosen method is straightforward in structure: building a prototype SMPS unit and testing it. The testing is divided into two sets. First set includes bench testing to evaluate the prototype PSU characteristics in comparison to the original PSU and the second set is testing in the full MEG system. The prototype replaces one of the original power supply units, to find the effect on noise levels of the actual MEG measurement. The procedures are explained in this chapter.

2.1 Building the SMPS unit prototype

The building of the prototype starts with defining the specifications. The specifications may not be exactly as in the original power supply e.g., for noise levels, but the other essential requirements are listed. To maintain reasonable schedule, the prototype unit is assembled by using commercially available SMPS modules instead of designing everything from the start. A specific self-made design would be more optimized in many ways, but it would take significantly more time and rigorous design work, which is not in scope of this study.

The identified essential requirements:

1. The SMPS modules must provide sufficient and stable DC outputs for the powered components.
2. The prototype must have suitable form factor and connections to be able to test it in the system.
3. SMPS modules must be isolated to provide similar level of patient and operator protection.
4. DC voltage and current output capability must be enough to pass the production tests defined for the original PSU.
   - +5 V dc, 4.55 A
   - ±15.5 V dc, 0.8 A

- ±6.6 V dc, 1.7 A

5. AC voltage input capability must cover the range of the original PSU.
   - 230 V ±10%, 50 or 60 Hz

The physical requirements are defined by dissecting the original power supply unit and taking measurements of the available space and how the connections could be made. It turns out that the original power supply PCB may be used as a connector base board by removing much of the large linear power supply components, line frequency transformer and large electrolytic capacitors. All SMPS modules and wiring should be able to fit in the freed-up space and connections can be made via the PCB to the original connectors. Figure 12 shows the fittings of the original linear power supply.

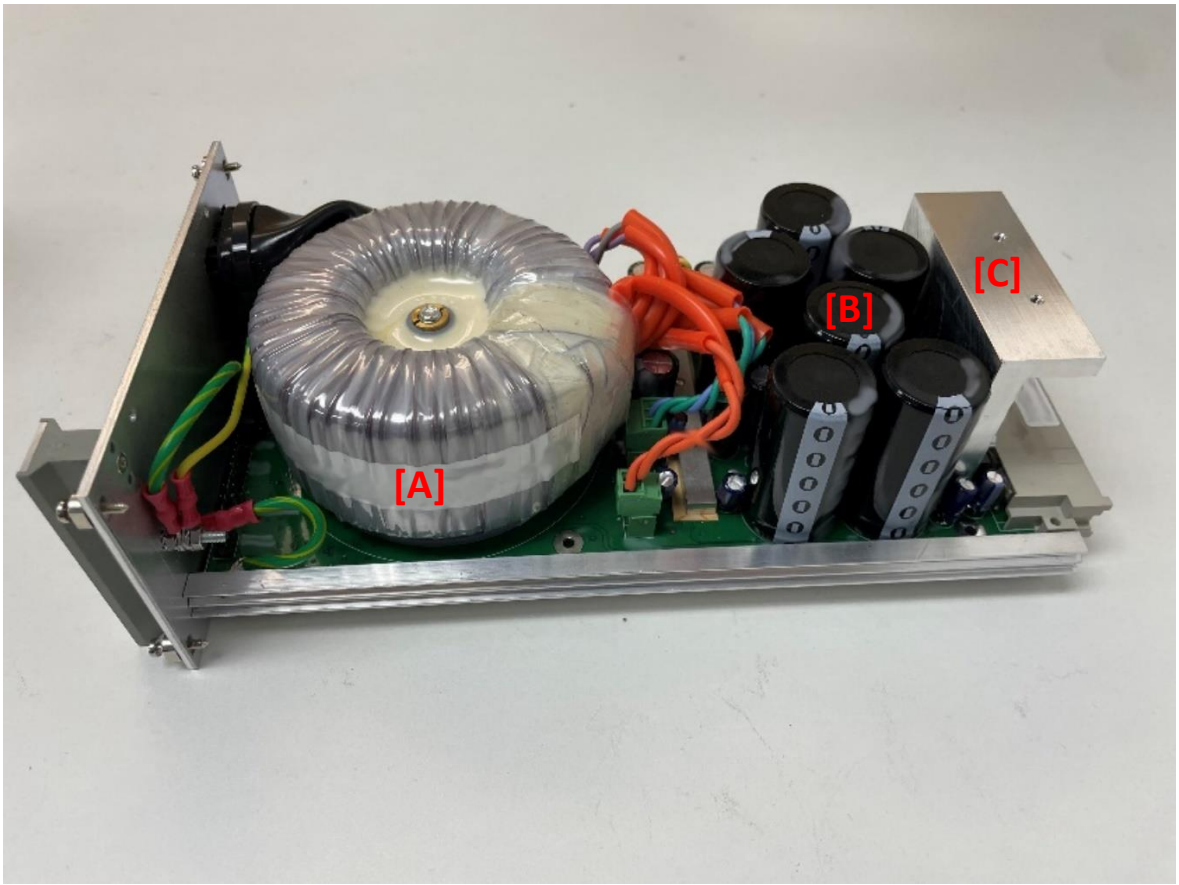

Figure 12. Original linear power supply. Inside of the enclosure: Toroidal line-frequency transformer with medical-level isolation [A], electrolytic capacitors after the rectifier [B], heat dissipation element attached to the regulating transistors [C].

After the specifications are clear, suitable SMPS modules must be found from trustworthy distributors and ordered. As the world situation is difficult for component availability, while doing this project, the range of suitable components that may be acquired in reasonable time frame is more limited than usual. Suitable selection can still be made with some alteration to the original intentions. Even though the essential requirements can be met, some headroom for suboptimal conditions is lost.

Now, there is not available a one SMPS module, which would have a single AC-DC rectifier section, and downstream, all required appropriate or adjustable output voltage DC-DC converters with suitable current handling capabilities. Suitable regulators for ±6.6 V for 2 A current were hard to get in time, so after careful assessment of the downstream components, it was replaced with two isolated 10 V regulators, the other one connected "upside down" providing the negative supply. As well, it was determined that rising the 5 V supply by 3.3 % is acceptable to adjust the dual 5 V & 15 V supply to 5.17 V & 15.5 V. The final power tree then consists of one dual output AC-DC converter (+5.17 V at 8 A, +15.5 V at 2.5 A), two identical single output DC-DC converters (10 V at 2 A) and an additional single output AC-DC converter (-15.5 V at 2 A) with switching frequencies of 70 kHz, 250 kHz, and 45 kHz respectively. The power tree is illustrated in figure 13.

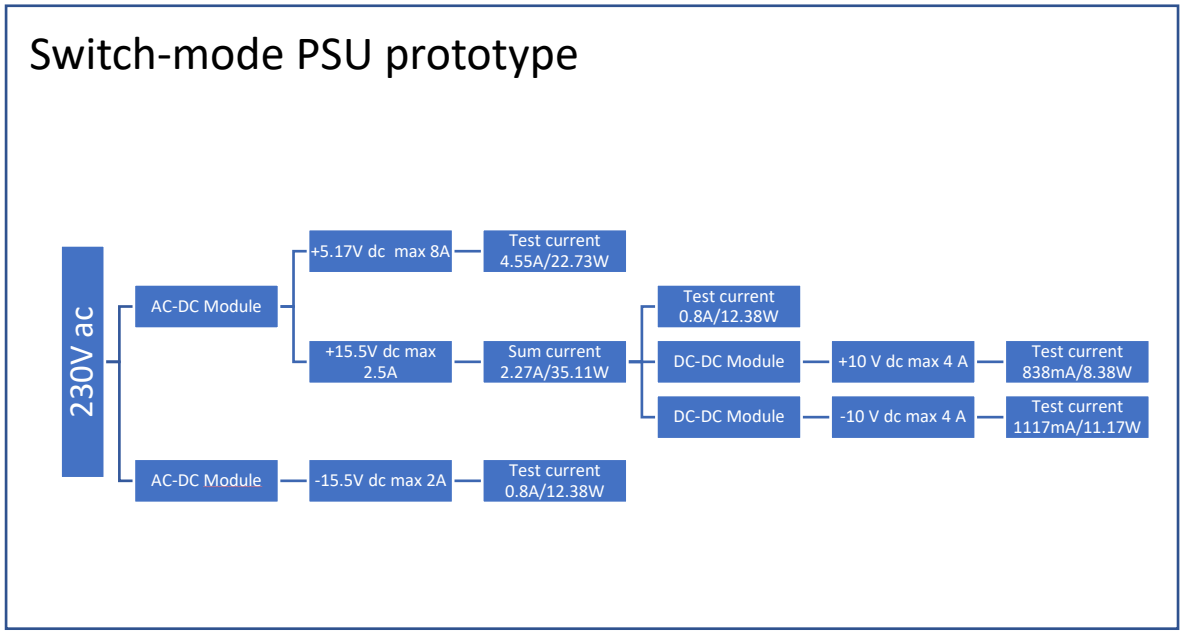

Figure 13. SMPS prototype power tree.

The assembling of the prototype begins by disassembling the original PSU to the point that new parts can be fitted inside. Transformer and large electrolytic capacitors are removed using a hand soldering iron. Initial placement for the SMPS modules is made and lengths of the wires, connecting the modules to the base board, are estimated. On the DC outputs, the module-end of the wires can be terminated with crimp connectors which are compatible with the acquired SMPS modules. Other ends of the wires are soldered to the base PCB, on the through hole pads of the removed output capacitors. The original connections from the utility input can be crimp terminated and connected to the AC input of the main AC-DC SMPS module. The protective earth connections to the enclosure and the base PCB are preserved. Figure 14 shows the fittings of the prototype power supply.

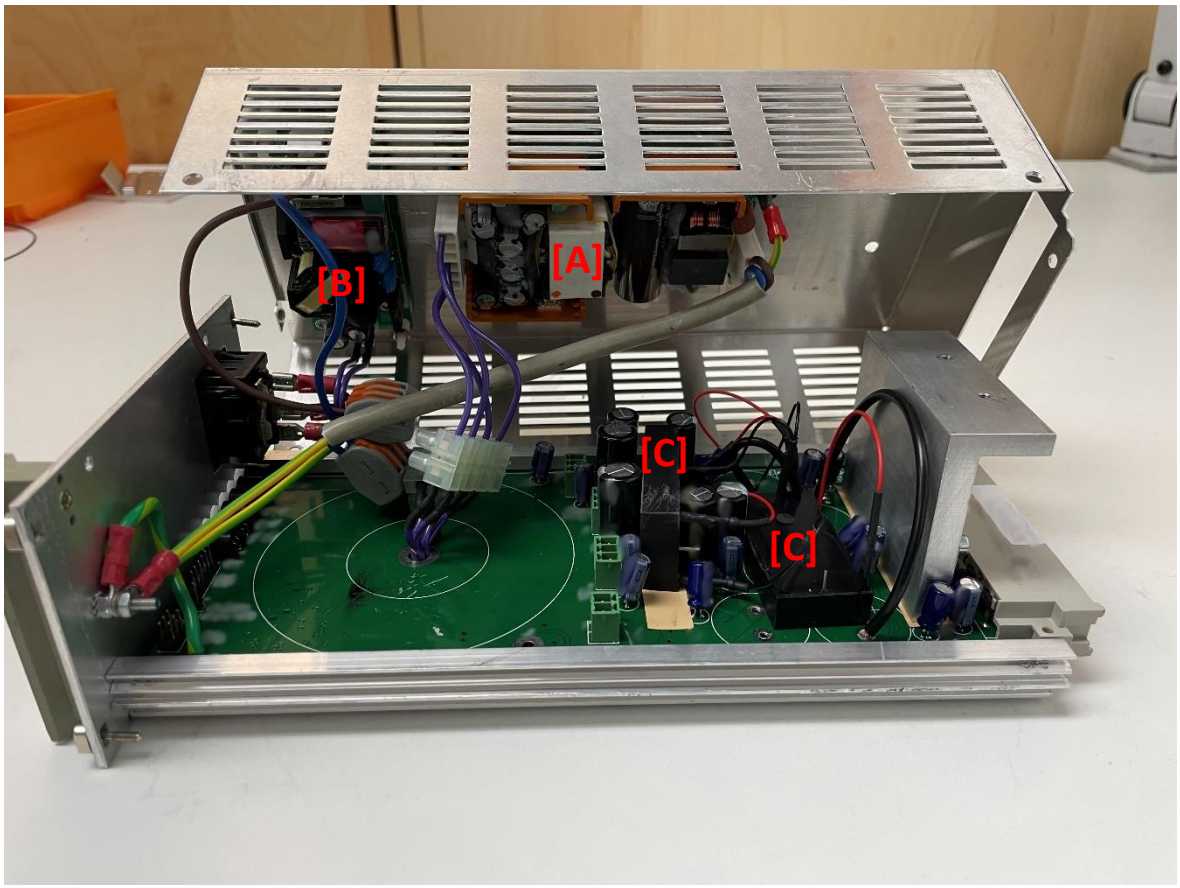

Figure 14. The SMPS modules inside the original enclosure. Dual output AC-DC converter attached to the cover [A], single output AC-DC converter attached to the cover [B], single output DC-DC converters attached to the PCB [C]

While fitting the modules inside the enclosure, care needs to be taken to ensure sufficient electrical isolation between conducting parts. Nonconducting stand-off screws are used to separate the SMPS modules from the aluminum enclosure. The wiring is placed carefully with no residue tension so the insulations remain intact, and the pressed connections may not slide off.

All the SMPS modules can be fitted inside the original enclosure with the connecting base board with almost no difficulty. Even the original power monitoring processor and over current switches can be made to work with the SMPS modules as well as the status LEDs indicating normal or faulty DC outputs.

2.1 Bench testing of the prototype

To learn about the characteristics of the SMPS prototype compared to the original PSU, both are first put through a series of oscilloscope measurements. The goal is to get a close view of the noise levels on top of the DC outputs. For this purpose, a special power rail probe is used. The power rail probe comprises of two signal paths that share the same probe tip, a high impedance path for accurate DC measurement and an additional 50-ohm path for the high frequency content. This allows us to find the low level, high frequency noise on the DC rails that cannot be seen very well with basic equipment. The probe, Keysight N7020A offers ± 850 mV dynamic range for the fluctuation over DC and the oscilloscope, Keysight DSOX4034A has 8-bit ADC. To balance between vertical clipping and resolution, the scale is set to 10 mV/div, full scale of 80 mV, yielding vertical resolution of 0.16 mV (Eq. 1) (Smith, 2020).

$$1/2\,LSB = 1/2 \times 0.08\,\mathrm{V} \times 1/2^8 \approx 0.16\,\mathrm{mV} \quad (1)$$

The measurement data is downloaded to PC in MATLAB format for further analysis, especially for the noise spectrum visualization with FFT function.

The first measurements are done with resistive loads to test the load regulation accuracy based on the original production test protocol. The output voltages should not drop below

suitable levels on maximal output currents. To consider the multiple outputs on the same power tree, all other outputs are loaded to higher than nominal output currents as well. The ripple on the DC output is measured with a bandwidth that covers the tens of Hertz, which is considered interesting in MEG, to the megahertz region, beyond the switching frequencies of the SMPS modules that might get aliased on the MEG measurement. The expected result is finding mostly 50 Hz rectifier-based noise with the linear power supply and additionally switching inherent noise with the SMPS prototype. Figures 15 and 16 show the measurement setup with a detached data acquisition rig.

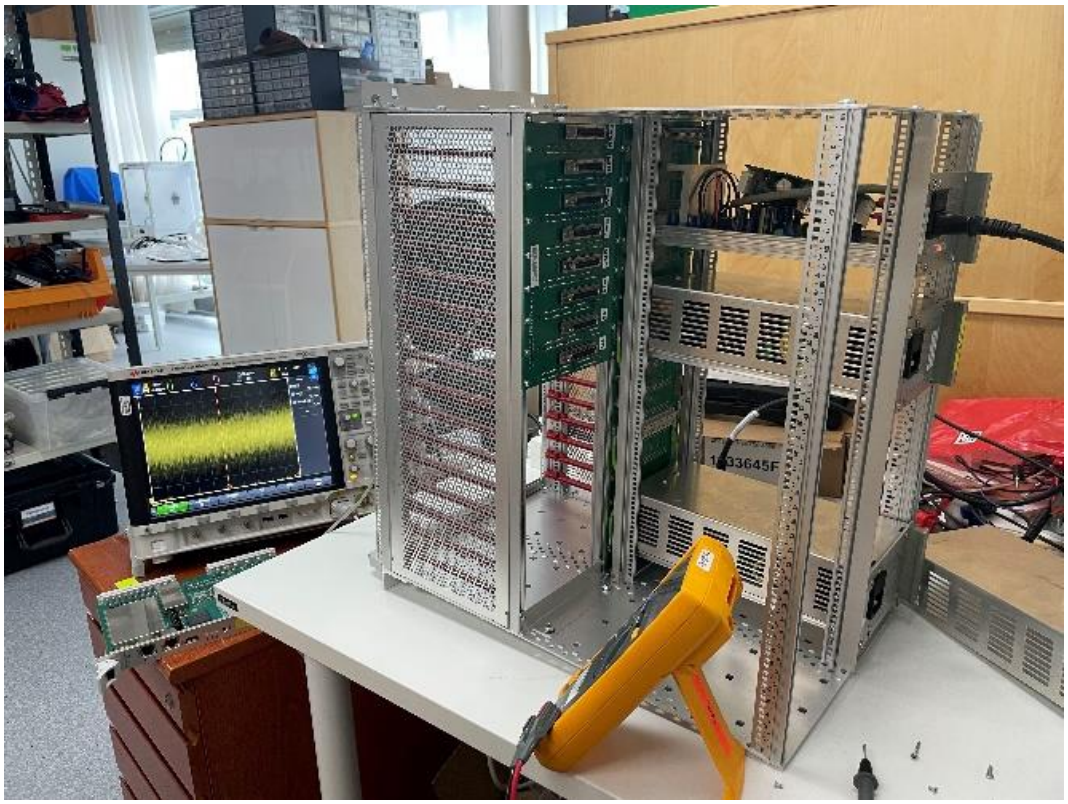

Figure 15. The bench testing setup. Prototype (top) and original power supplies tested side by side.

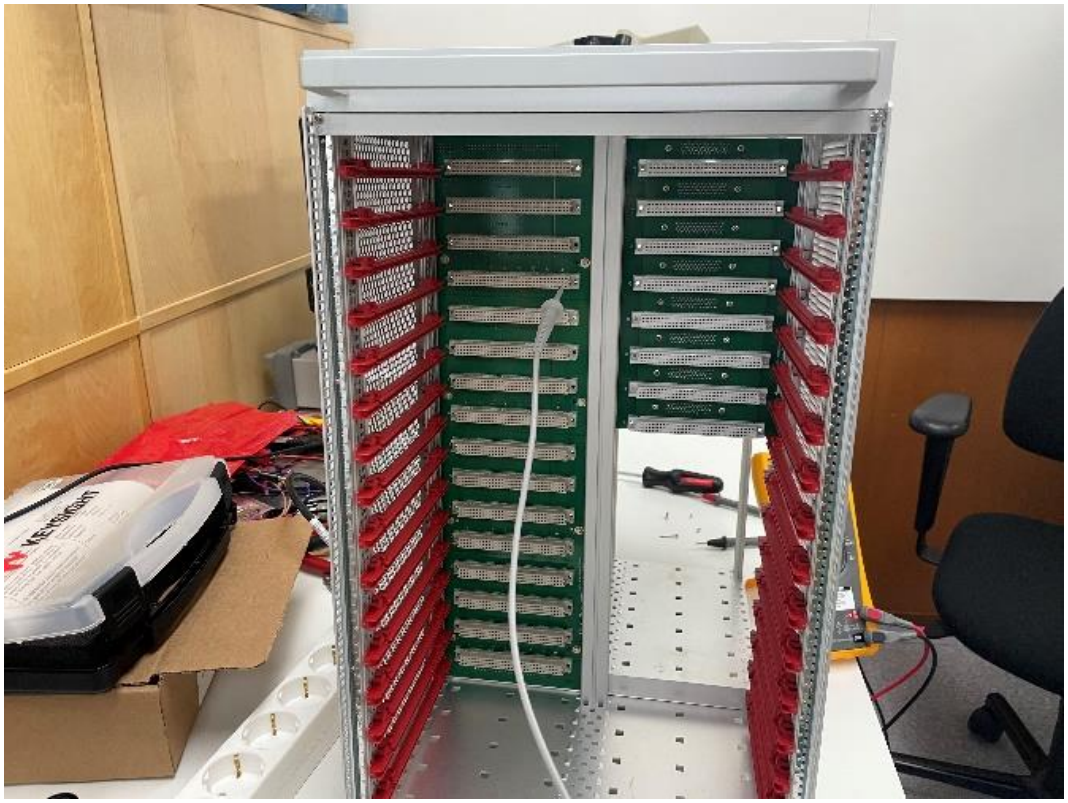

Figure 16. Oscilloscope probe attached directly to a connector slot.

The second phase of the bench testing involves one data acquisition board powered by the power supply under test. The power rail measurements are done with maximum frequency band to find out the effect of the high-speed electronics running on the board. These measurements may also serve as product development information for the data acquisition board itself. The expected result is finding additional high-speed data interface originated noise which propagates through the power rails.

2.2 Testing in the MEG system

The full system noise test is agreed to be done in the production facility where similar tests are done to all customer systems before shipping. The initial intention was to use Megin's own product development system, but due to the office relocation at the time, the system is not in fully operable state. To be sure that no harm is caused to the delivered system by the prototype power supply, it is "smoke tested" in less risky environment first and gradually move towards the actual system.

The first step is already taken in the oscilloscope measurements while using one data acquisition board as a live test load. From these measurements, it should already be noticeable from the voltage rail fluctuations that the board is on live state and the software has not hanged due to unstable power supply for the processing units.

The second step is to use a software development rack with a similar data acquisition board. This time, using a serial terminal connection to interact with the embedded software, it can be checked from the self-monitoring functions that the internal voltages on the board show appropriate readings and more generally, that the software boots up and runs normally.

Third step is applying the prototype power supply in the product development system, while in not fully operable state at the time, it can still be powered up and the relevant self-monitoring readings can be accessed. Different from the previous step, the prototype is now running as a part of the full system. It powers up several data acquisition boards, all live and running the embedded software, though meaningful MEG measurements cannot be performed.

Finally in the fourth and final step of the system testing, if all previous tests have been passed, with nothing suspicious happening, there should be enough evidence that no harm is probable to the system in production and the system noise tests can be performed with the prototype power supply. The testing flow chart is presented in figure 17.

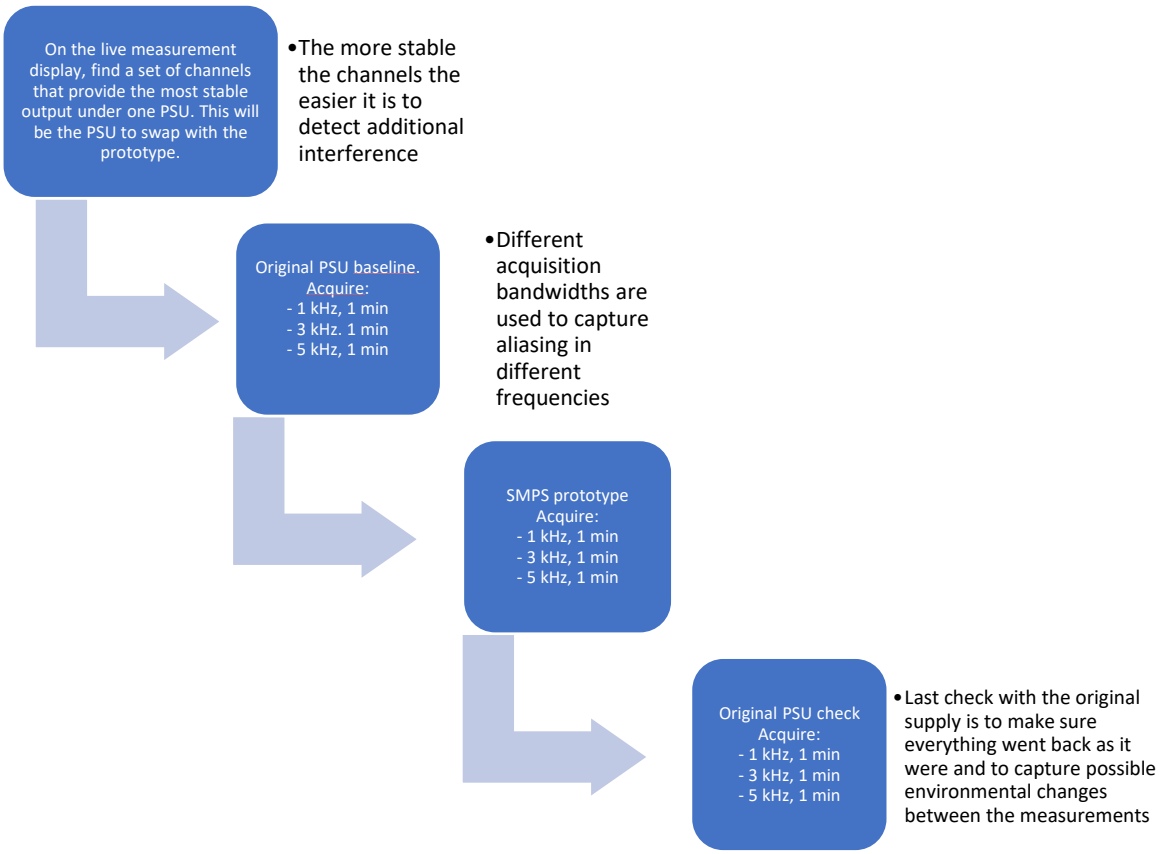

Figure 17. The MEG noise test flow chart

The acquired MEG measurement data is downloaded from the acquisition workstation for further analysis. The data is analyzed with proprietary software tools developed at Megin to assess the possible noise issues at customer sites and for product development. The data can also be extracted in MATLAB format and accessible down to single samples if closer inspection or development of different kinds of analyses are needed.

3 Results

This chapter presents the results of the measurements described in the previous chapter. The oscilloscope data in MATLAB format is analysed and graphically visualized. The MEG data is visualized using Megin's own analysis software. The objective is to find meaningful differences between the Linear and the SMPS results to conclude if using the SMPS degrades the MEG performance significantly, catastrophically or at all and if the findings from the power rail measurements support the conclusion.

3.1 Bench testing

The first set of measurements are based on the production test specification of the original power supply for applicable parts. These include load regulation and ripple characteristics. The load regulation is presented in table form and the ripple waveforms and spectra are presented in graphical form.

3.1.1 Load regulation test

Load regulation test is used to determine if the output voltage of the regulator stays within specified range in expected load conditions using a resistive load. The conditions listed below come from the production test specification. An electronic load is used in constant current mode to set the test load with 1 mA accuracy. Outputs, other than the one being tested, are loaded with a power resistor array with higher than nominal current to provide necessary minimum load and to consider the cross regulation in the dual-output SMPS module. Test specifications are listed in table 1.

Table 1

Output	Test current	Pass criteria
+15.5 V	800 mA	> 15.1 V
-15.5 V	800 mA	< -15.1 V
+6.6 V	1.27 A	> 6.5 V
-6.6 V	1.69 A	< -6.5 V
+5 V	4.55 A	> 4.9 V

In the SMPS prototype, the ±6.6 V outputs are replaced with ±10 V outputs, so the test currents are adjusted to equivalent power (table 1, continued).

Table 1 (continued)

Output	Test current	Pass criteria
+10 V	838 mA	> 9.9 V
-10 V	1117 mA	< -9.9 V

Table 2: Linear power supply results

Output	Voltage with nominal load	Voltage with test load	Deviation
+15.5 V	15.512 V	15.508 V	-0.004 V
-15.5 V	-15.543 V	-15.541 V	-0.002 V
+6.6 V	6.612 V	6.603 V	-0.009 V
-6.6 V	-6.633 V	-6.630 V	-0.003
+5 V	5.018 V	5.008 V	-0.01 V

Table 3: SMPS prototype results

Output	Voltage with nominal load	Voltage with test load	Deviation
+15.5 V	15.653 V	15.594 V	-0.059 V
-15.5 V	-15.619 V	-15.606 V	-0.013 V
+10 V	10.028 V	10.029 V	0.001 V
-10 V	-10.026 V	-10.026 V	0 V
+5 V	5.160 V	5.138 V	-0.022 V

Test results listed in table 2 and 3 show that the SMPS prototype passes the load regulation tests. Especially the ±10 V regulators seem to be practically unaffected by the approximately 50 % of the regulators rated loading.

3.1.2 Voltage ripple test

The output voltage ripple is measured with an oscilloscope. The data is collected in MATLAB format for visualization and analysis. The requirement for ripple, set in the production test specification, is 1 mV peak-to-peak at line frequency for all outputs. This requirement is purposefully overlooked, and the focus is in covering the noise spectrum to the MEG band of 5 kHz for head-to-head comparison and the switching frequencies and harmonics are inspected separately in higher frequency band.

Corresponding outputs of the Linear PSU and the SMPS prototype are compared in time domain and frequency domain focusing on the MEG band. Oscilloscope measurements are conducted in 10 MSPS sampling frequency in digitization mode, full scale of 80 mV with no averaging or waveform holding. Time domain measurement DC values are set off to fit waveforms in same graph and scale. Following figures show examples of different measurement and analysis types. More measurement graphs are collected in Appendix 1.

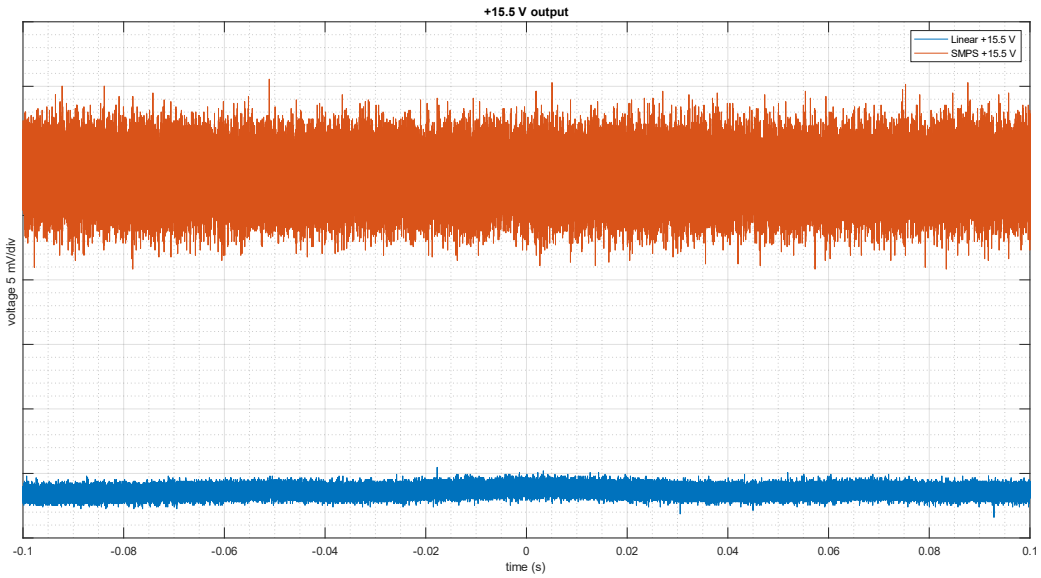

Figure 18. +15.5 V comparison in time domain.

Figure 18 shows the comparison of SMPS and linear power supply ripple in time domain. The linear output fluctuation is around 2 mV peak to peak, whereas in the switch-mode output it is around 15 mV peak to peak.

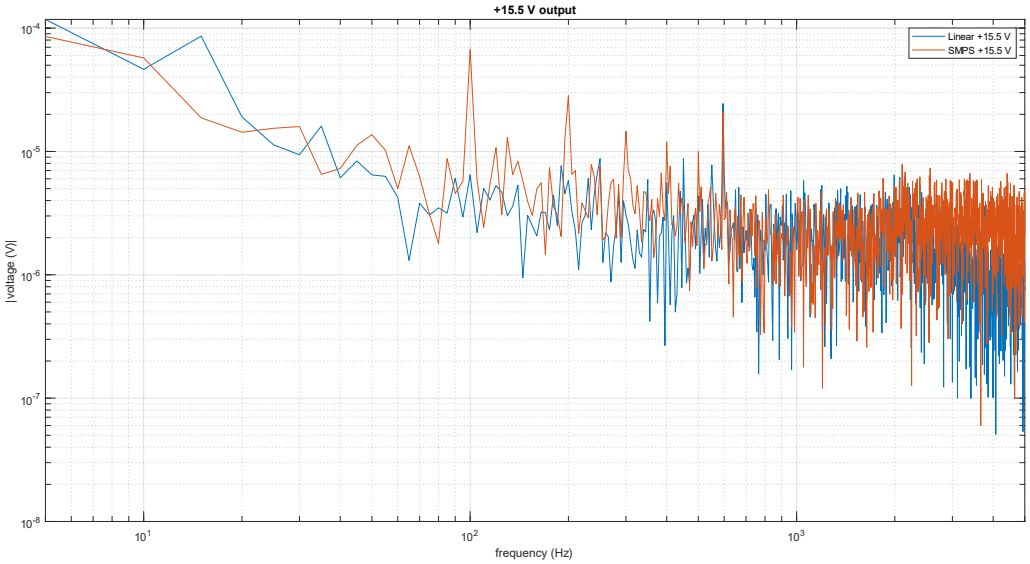

Figure 19. +15.5 V comparison in frequency domain, MEG band

Figure 19 shows the comparison in frequency domain at the “MEG band” of dc to 5 kHz. Some differences can be seen e.g., the line frequency harmonics seem to be lower in the linear power supply. This may be the result of putting lots of effort in filtering the line frequency harmonics in the original power supply design.

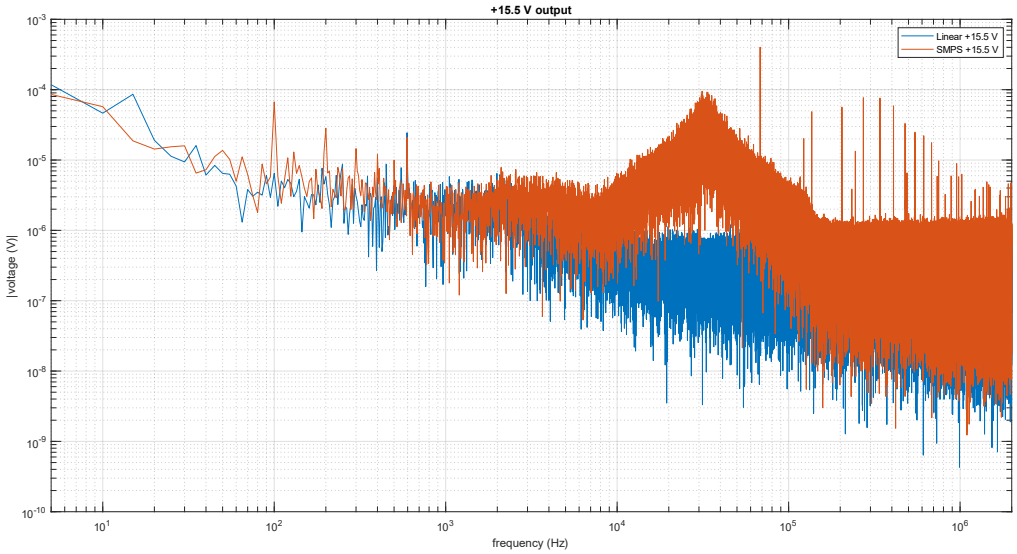

Figure 20. +15.5 V comparison in frequency domain, medium band

Figure 20 shows the comparison in the “medium band”, that is extended to 2 MHz to see the effects of SMPS switching activity. The difference becomes very prevalent up from the tens of kHz and the switching frequency of 70 kHz and its multiples can be clearly distinguished.

3.1.1 Active load measurements

The second phase of the oscilloscope measurements use a single data acquisition board as an active load. Higher bandwidth is used to capture the effects of the high-speed interfaces on the board.

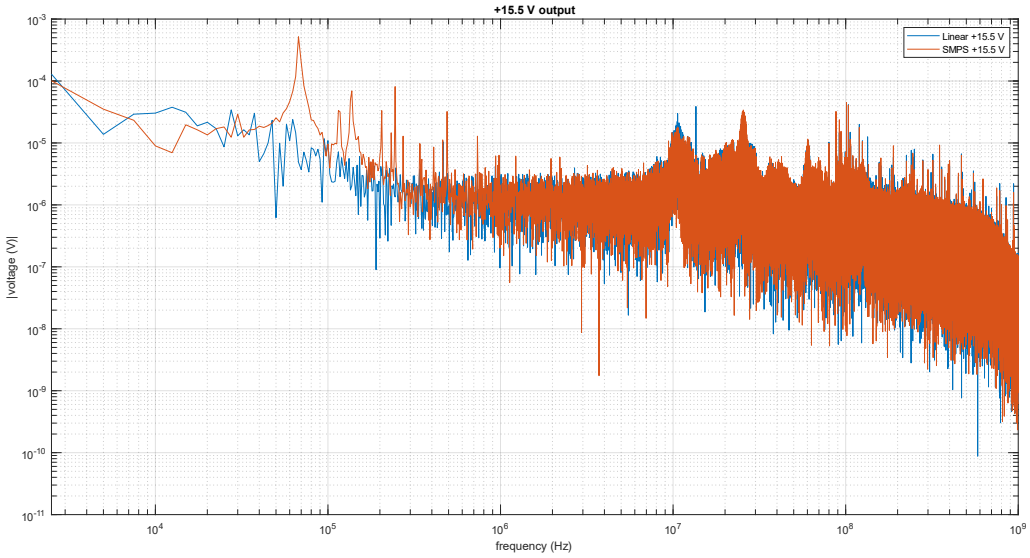

Figure 21. +15.5V comparison with active load, high frequency

Figure 21 shows the high frequency band extending to 1 GHz with an active data acquisition board powered up by the power supplies. From the tens of MHz up, the spectrum starts to seem similar between the two power supplies. At this region, other sources of electromagnetic emissions such as cross coupled high-speed interfaces and oscilloscope noise start to dominate.

3.2 MEG system testing

This section presents the results of the tests where the SMPS prototype is attached as a part of the MEG system. The testing starts cautiously with smoke testing of a small part of the system and proceeds gradually towards a fully functional system to be sure that no damage done to the expensive equipment.

3.2.1 Self-monitoring test

System testing begins with the SW-development rack test. In this test, the SW-development rack, fitted with one data acquisition board is powered up by the prototype PSU. The data acquisition board is then interfaced with serial terminal connection to query the internal

voltage monitoring function. The data acquisition board should output correct voltages to the terminal. This way it is clear that the embedded software is alive and not hanged because of unstable power supply or other disturbances in the digital signalling.

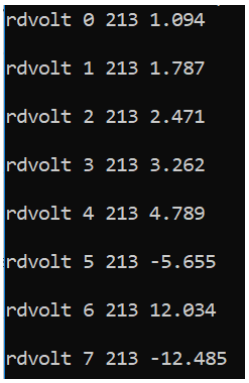

Figure 22. Resulted output from the internal voltage monitoring

The output at figure 22 looks as expected and so we can be sure that the software is active on the board, and no unexpected failure has happened.

3.2.1 MEG noise tests

The MEG noise tests are performed as described in the Methods chapter. The data is collected in the manufacturing premises with a complete system. The MEG noise spectrum graph types are introduced here, and the rest of the complete collection can be found in the Appendix 2.

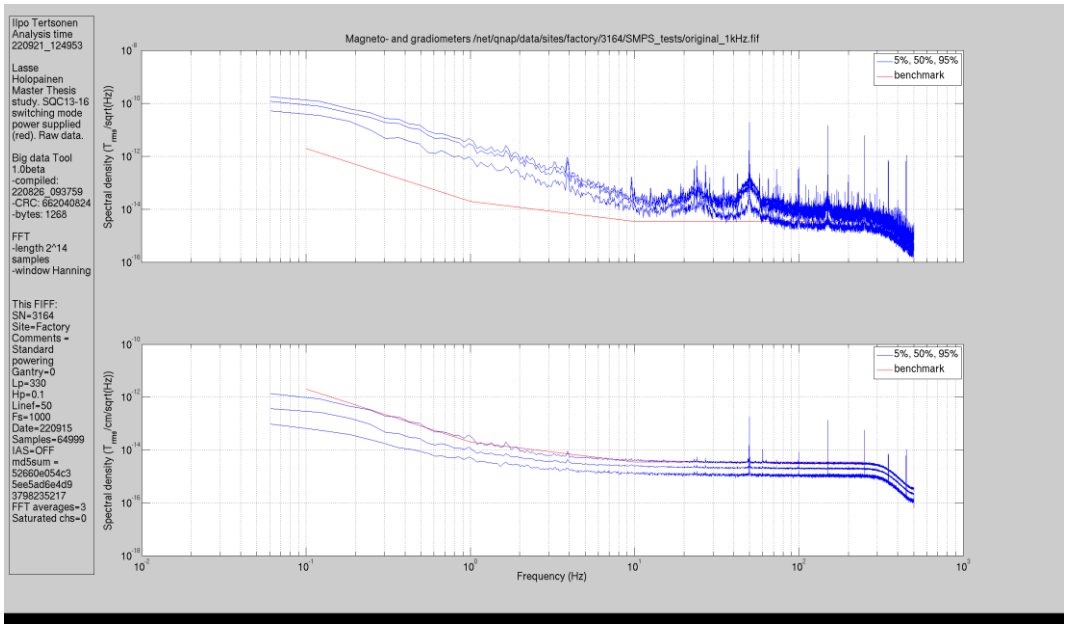

Figure 23. Noise spectrum: Original PSU

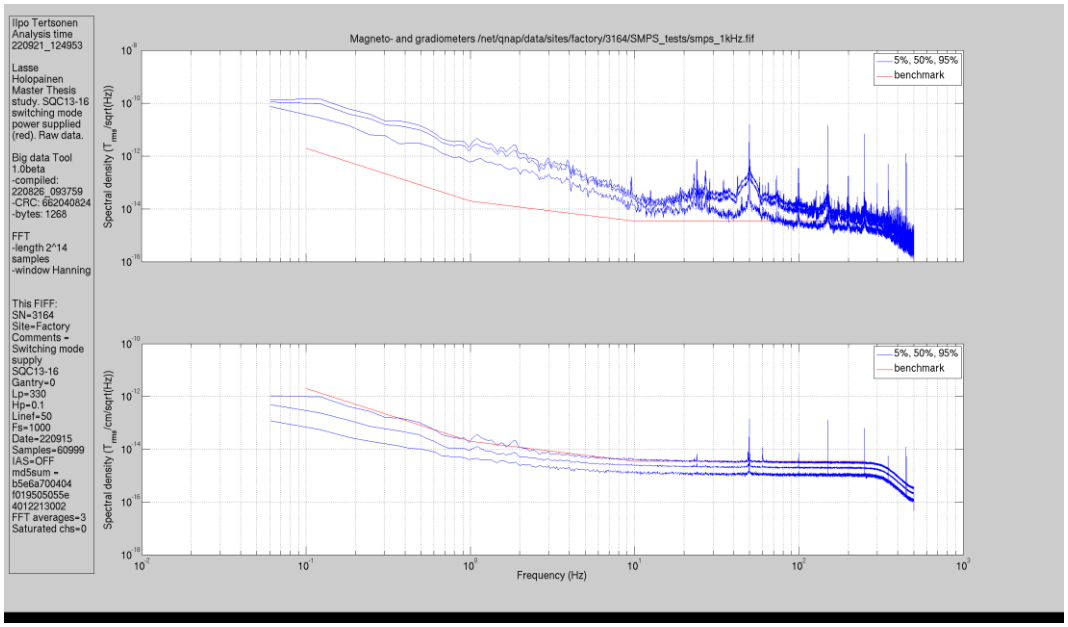

Figure 24. Noise spectrum: Prototype PSU

Figures 23 and 24 present the first output graph type from Megin's noise evaluation tool. The graph presents an FFT of the combined MEG empty-room data from the set of four data acquisition boards powered with either the original linear power supply (Fig. 21) or the SMPS prototype (Fig. 22). All other 28 boards of the data acquisition system are powered with the original linear power supply. The data set is collected with 1 kHz

sampling frequency and the span of the spectrum is from 0.5 Hz to 500 Hz. Low-pass filter is applied with the corner-frequency at 330 Hz and high-pass filter at 0.1 Hz. The graphs can be compared side by side to determine if there are differences in the frequency content or amplitude. The red line titled “benchmark” is an arbitrary reference for easier perception of scale. At glance, it seems there is no notable difference between the power supply types.

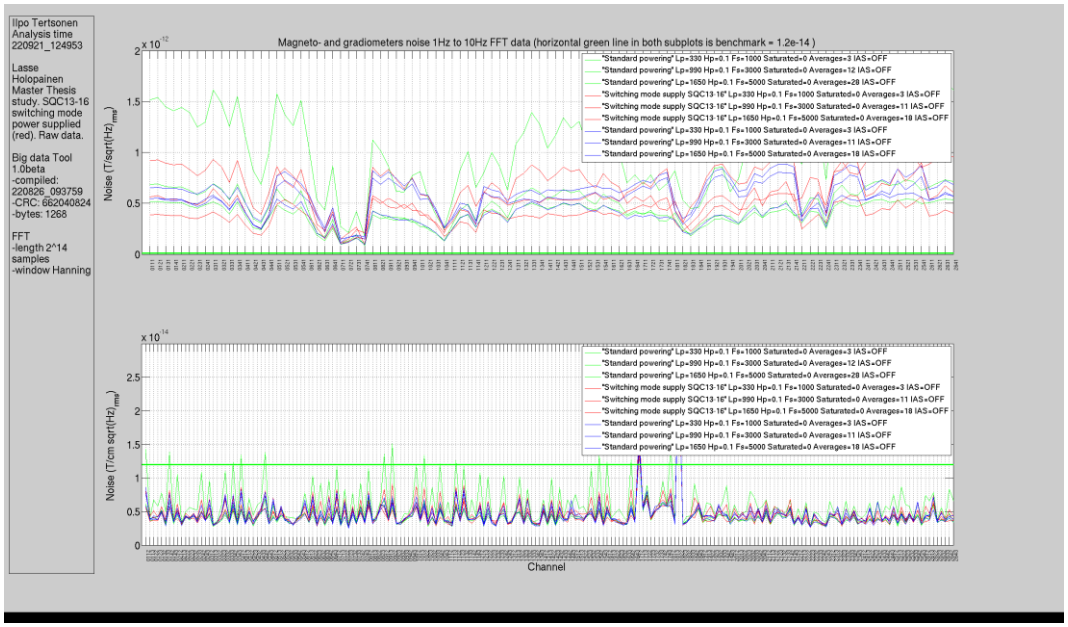

Figure 25. Noise FFT data

Figure 25 presents the low frequency noise values in channel-by-channel basis. The different colours represent the different power supplies used during the tests; green lines are the first tests with the original PSU, red lines are the prototype PSU, and blue lines are the original power supply returned for control, all at 1, 3 and 5 kHz sampling frequencies. Top graph is for magnetometers and bottom graph is for gradiometers. There seems to be more differences between first and second rounds with the original PSU than there is between the original and the prototype PSUs. The differences in the graphs are better explained with environmental changes between different test rounds rather than the difference of the PSUs.

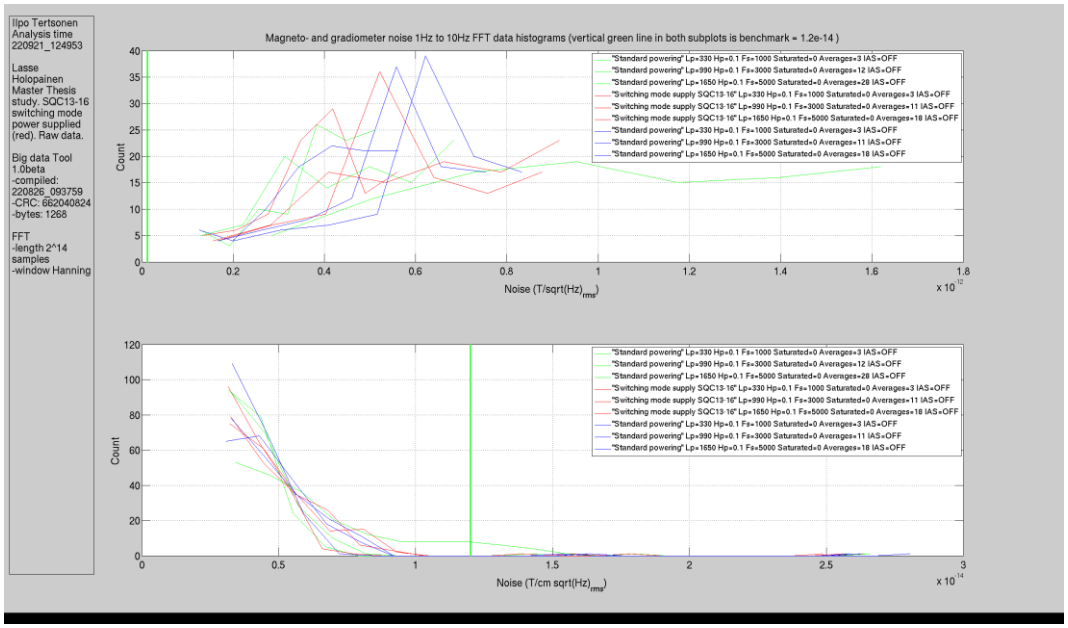

Figure 26. FFT data histograms

The histograms of the previous data are presented in figure 26. The individual data samples are counted by their noise levels to see how the values are distributed over the data set. Again, there seems to be more difference between the test runs than between PSU types, likely explained by environmental changes.

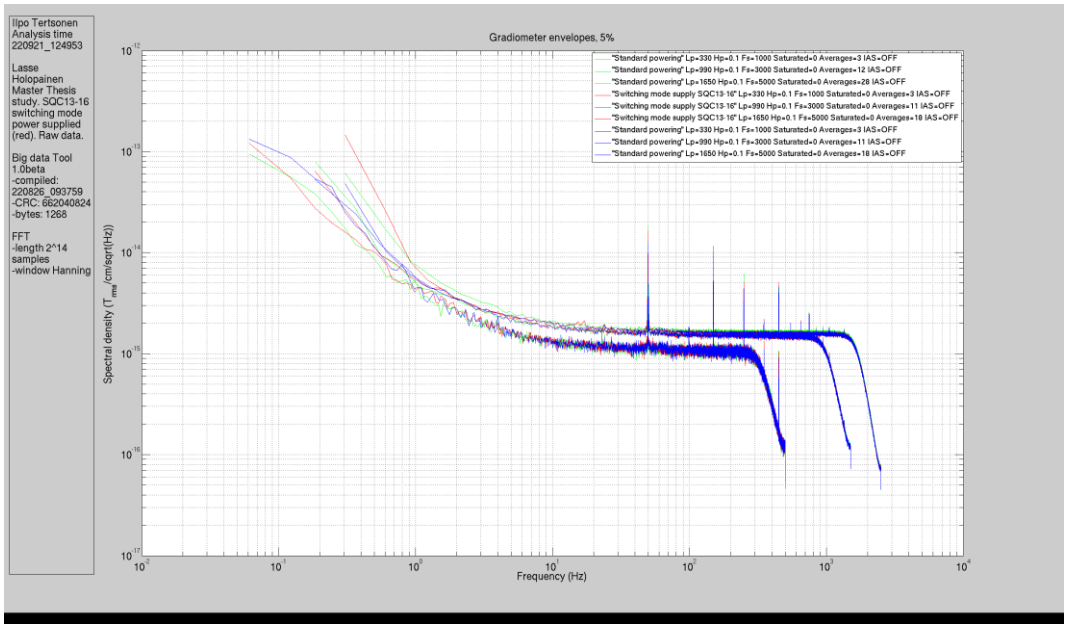

Figure 27. Spectral density gradiometers

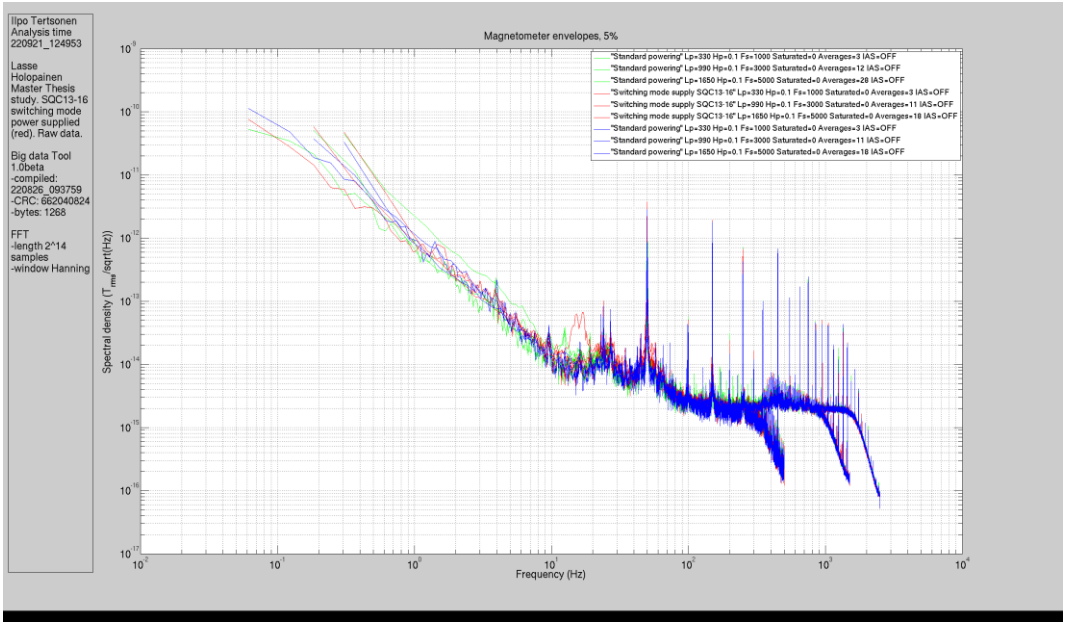

Figure 28. Spectral density magnetometers

Figures 27 and 28 present all test runs combined for gradiometers and magnetometers separately. Here, the graphs seem quite similar with mostly minor differences one way or the other between original and prototype PSUs. One notable point in the graph is in one of the prototype power supply runs, between 10 to 20 Hz. The extremely low frequency of the “glitch” may indicate some mechanical vibration during the test, but to be sure, it should be confirmed by retesting.

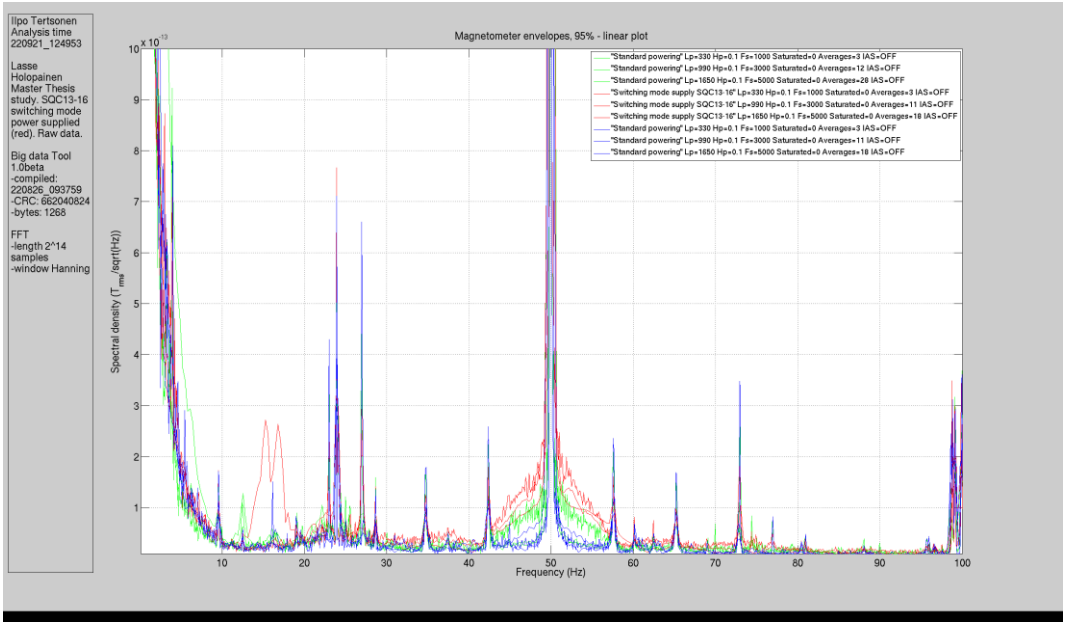

Figure 29. Spectral density magnetometers, linear

The final graph type from the noise evaluation tool is presented in figure 29, which shows the data from the previous graph of magnetometers in a linear frequency axis from 0 to 100 Hz. Here the low-frequency glitch mentioned before is visible at around 15 to 17 Hz, and it seems that the red prototype PSU lines are consistently slightly higher, especially visible around the 50 Hz line-frequency spike in the middle. Comparing visually to the deviation on the other test runs, the difference might be insignificant, but it should be inspected further to be sure.

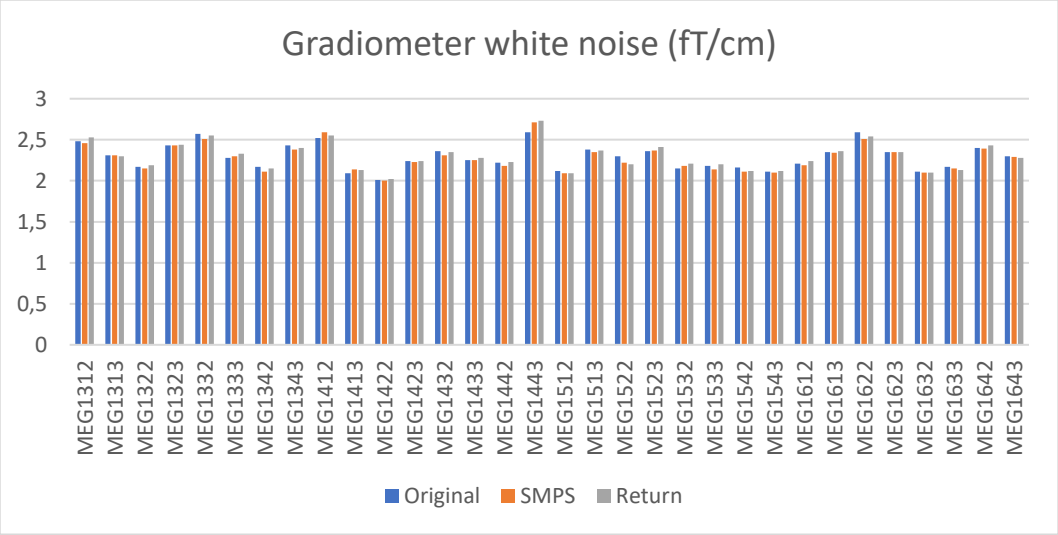

Figure 30. Gradiometer white noise levels

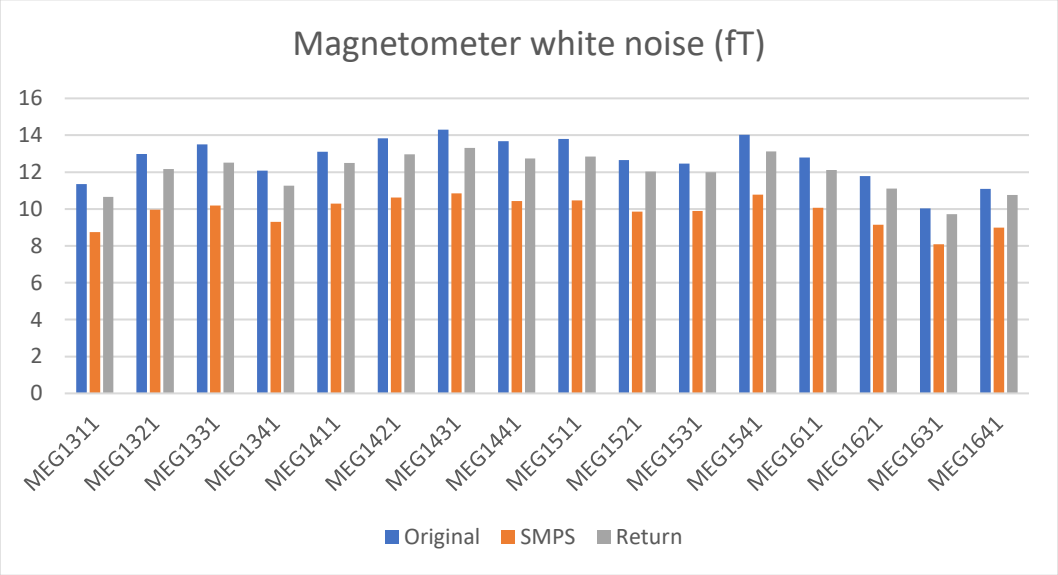

Figure 31. Magnetometer white noise levels

Figures 30 and 31 present the white noise levels at 800 Hz to 900 Hz band calculated from the 5 kHz sampling frequency test runs. These values are used to quickly evaluate and compare the quality of the system and the installation environment. For the gradiometers, the white noise levels seem to be quite unchanged between the power supplies. In the magnetometer levels, it even seems like the noise levels are consistently lower in the SMPS prototype test run.

4 Conclusions

The final concluding chapter reflects the study and forms an answer to the research question; are the switch mode power supplies a feasible technology to be used in the MEG system? The study did not find clear noise performance degradation on the MEG measurement, even though the effects of the SMPS operation were evident in the DC-voltage rails and the prototype power supply was not at all optimized to the purpose. The study considered only powering of the digital data acquisition hardware, and the stretch opportunity of testing the SMPS also in the analog front end was not yet taken. The analog front-end testing would be a reasonable following step in evaluating the technology.

The results of the study were presented to the senior MEG system experts and the possible continuation of the SMPS technology evaluation with further testing were discussed.

The methods chosen to answer the research question were building a prototype SMPS unit and testing it against the specifications of the original linear power supply and functionally with the system. The methods aimed to provide information about how the switching related noise affected the DC-voltage rails on the digital data acquisition hardware and whether the additional noise, in the end, affected the noise levels on the actual MEG measurements. The methods succeeded in providing credible evidence that the noise performance of the MEG system was not affected considerably by the standard noise performance criteria. There should still be more testing and evaluation before the SMPS technology could be considered in the product roadmap. Similar testing methods could be applied for the analog front-end measurements by replacing a front-end linear power supply with a suitable SMPS prototype.

The test results include oscilloscope measurements for DC-rail noise, functional testing, and noise measurements with the MEG system. The oscilloscope measurements, transformed to frequency domain, show the obvious increase in noise in the typical SMPS operating bands. There doesn’t seem to be significant difference in the noise amplitudes between linear and SMPS in the MEG operating band of 0 to 5 kHz, though there would still be possibility of high frequency noise aliasing on the MEG measurement data. In the much higher frequencies, beyond the most significant SMPS switching harmonics, other noise sources such as high-speed digital interfaces and omnipresent radio transmitters

possibly dominate the spectrum, and the difference between linear and SMPS becomes ambiguous. The functional test results with digital electronics didn't show any problems with the digital processing systems, which would have disrupted the software either in the idle state on the first smoke tests or in the actual data acquisition state while measuring the noise. The MEG noise test results give an impression of relatively well performing system with no significant deviation of performance between linear and SMPS. Sampling frequencies of 1, 3 and 5 kHz were used to consider the possible aliasing effect.

The analysis of the measurement data was performed by observing the difference in the visual representation of linear and SMPS data. The raw time domain data from the oscilloscope was downloaded to PC in MATLAB format. A MATLAB script was written to transform the time domain data to frequency domain with an FFT function and plot the result in base 10 logarithmic x- and y-axes. The FFT spectrum analysis used here is not as precise as a sweep spectrum analysis would have been in terms of frequency resolution and dynamic accuracy. The frequency range of the FFT analysis is determined by the sampling frequency of the oscilloscope and the frequency resolution depends on the length of the time domain record. With the equipment at hand, the maximum frequency component is theoretically 2.5 GHz at Nyquist rate and the frequency resolution 5 Hz, which is deemed good enough for the purpose. The relevant and expected spectral components can be observed from the presented three different frequency bands. The MEG noise measurement results are analysed with proprietary tools from Megin Oy. The analysis tools give MEG system specific graphical information about the noise performance, channel-by-channel and by sensor type. This makes the results comparable with all the other similarly recorded noise evaluation data sets. The visual comparison between linear and SMPS data is also straightforward with the output graphs from Megin's analysis tools. There's also a numerical white noise value calculated from the data for each sensor, which is comparable between different data sets. It was not covered in this study, but there would also be possibility to extract all the MEG measurement data in numerical form and develop new analysis tools for example in MATLAB or Python script, if deemed useful.

The higher motivation for this new technology evaluation is altogether replacing the, in many ways inefficient line frequency linear power supplies in the system with switch-mode power supplies. This study considered just the powering of the digital data acquisition hardware and there are still other subsystem parts powered with the same kind

of linear power supplies. To replace them all with SMPS units or even a combined larger unit, all the subsystems' possible performance degradation should be carefully examined. Rethinking the power supplies of the whole system is a laborious task with wide technical and compliance aspects, but there is potential for cost reduction, production scalability and new technological opportunities.

References

Bykhovsky D (2022) Experimental Lognormal Modeling of Harmonics Power of Switched-Mode Power Supplies. *Energies* 15(2).

Cohen D (1972) Magnetoencephalography: Detection of the Brain's Electrical Activity with a Superconducting Magnetometer. *Science* 175(4022): 664-666.

Cohen D (1968) Magnetoencephalography: Evidence of Magnetic Fields Produced by Alpha-Rhythm Currents. *Science* 161(3843): 784-786.

Gunawardane K, Padmawansa N, Kularatna N, Subasinghage K, Lie TT (2022) Current Context and Research Trends in Linear DC–DC Converters. *Applied Sciences* 12(9): 4594.

Hämäläinen M, Hari R, Ilmoniemi RJ, Knuutila J, Lounasmaa OV (1993) Magnetoencephalography—theory, instrumentation, and applications to noninvasive studies of the working human brain.

Health Canada (2023) *List of Recognized Standards for Medical Devices.*

Heikkilä, M. (2014) Kylmätutkimus Raivasi Tien Aivoihin. *Tekniikan Historia 4.6.2014.* Helsinki: Alma Talent Oy.

Iqbal MN, Kütt L, Asad B, Vaimann T, Rassõlkin A, Demidova GL (2020) Time Dependency of Current Harmonics for Switch-Mode Power Supplies. *Applied Sciences* 10(21).

Leferink F and Roc'h A, (2011) Analysis of Common Mode Inductors and Optimization Aspects. In*: Anonymous* , 3-37.

Manjunath A, Sudheer ML (2020) Mitigation of CM conducted EMI in flyback converter using balancing capacitors. *IET Power Electronics* 13(19): 4572-4580.

Megin Oy archives (1989) *Osakassopimus SITRA:n ja Instrumentarium Oy:n ja Mustekala Ky:n välillä 9.6.1989*

Mohan N, Undeland TM , Robbins WP, (2003) *Power Electronics : Converters, Applications and Design.* Hoboken (NJ): Wiley.

Ott HW (1988) *Noise Reduction Techniques in Electronic Systems.* New York: Wiley.

Rashid MH (2011) *Power Electronics Handbook Devices, Circuits, and Applications.* Amsterdam ;: Elsevier/BH.

Smith K (2020) *Understanding Voltage Measurement Accuracy for InfiniiVision Oscilloscopes.* Retrieved [May 21, 2023] Available at: https://edadocs.software.keysight.com/kkbopen/understanding-voltage-measurement-accuracy-for-infiniivision-oscilloscopes-584425356.html.

Subotskaya V, Bodano E, Deutschmann B (2020) EMI-optimized driver for high-frequency boost converter. *E & i Elektrotechnik Und Informationstechnik* 137(2): 100-106.

The European Parliament and the Council of The European Union (2017) *Regulation (EU) 2017/745 of the European Parliament and of the Council, Official Journal of the European Union L117 (5.5.2017).*

Tierney TM, Holmes N, Mellor S, López JD, Roberts G, Hill RM, Boto E, Leggett J, Shah V, Brookes MJ, et al. (2019) Optically pumped magnetometers: From quantum origins to multi-channel magnetoencephalography. *NeuroImage* 199: 598-608.

U.S. Food & Drug Administration. *Medical Devices, Recognized Consensus Standards*. Retrieved [May 31, 2023] Available at: https://www.accessdata.fda.gov/scripts/cdrh/cfdocs/cfstandards/search.cfm

Zimmerman JE, Thiene P, Harding JT (1970) Design and Operation of Stable rf-Biased Superconducting Point-Contact Quantum Devices, and a Note on the Properties of Perfectly Clean Metal Contacts. *Journal of Applied Physics* 41(4): 1572-1580.

Appendix 1. Ripple analysis graphs

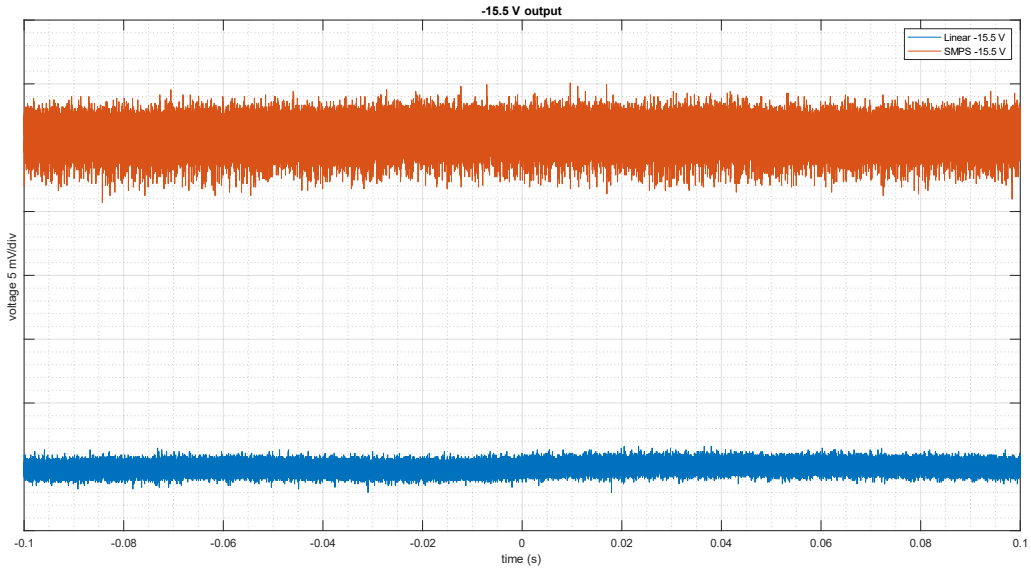

Figure A1.1. -15.5 V comparison in time domain

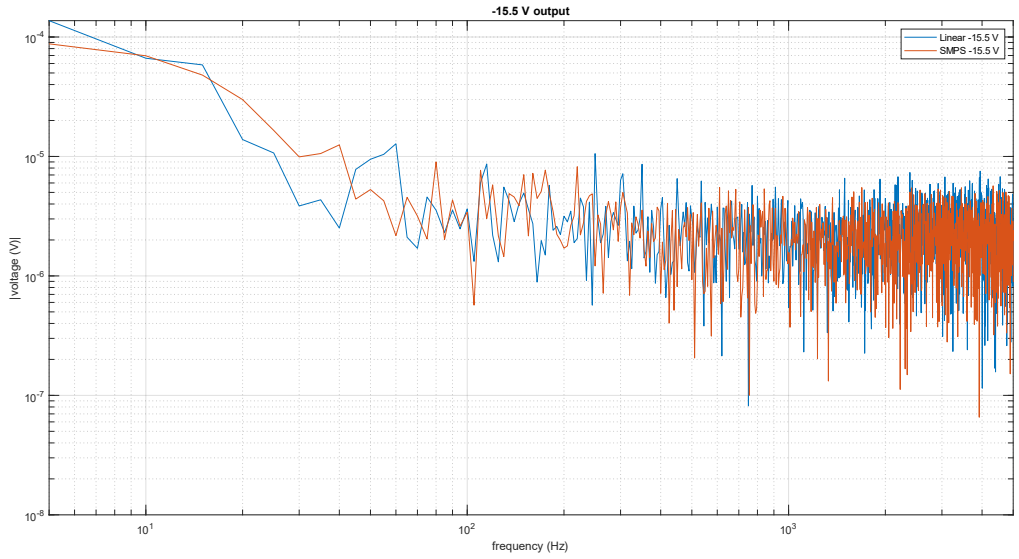

Figure A1.2. -15.5 V comparison in frequency domain, MEG band

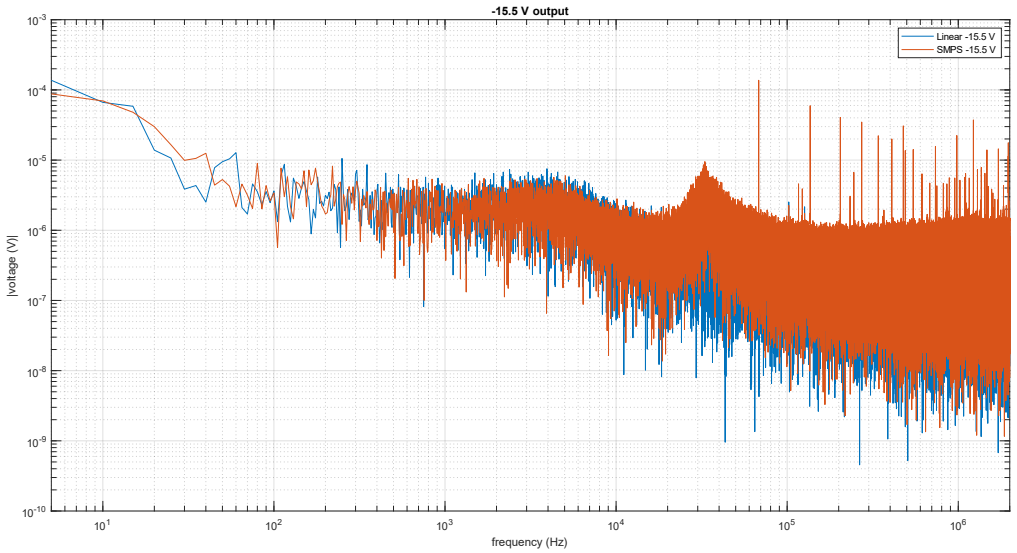

Figure A1.3. -15.5 V comparison in frequency domain, medium band

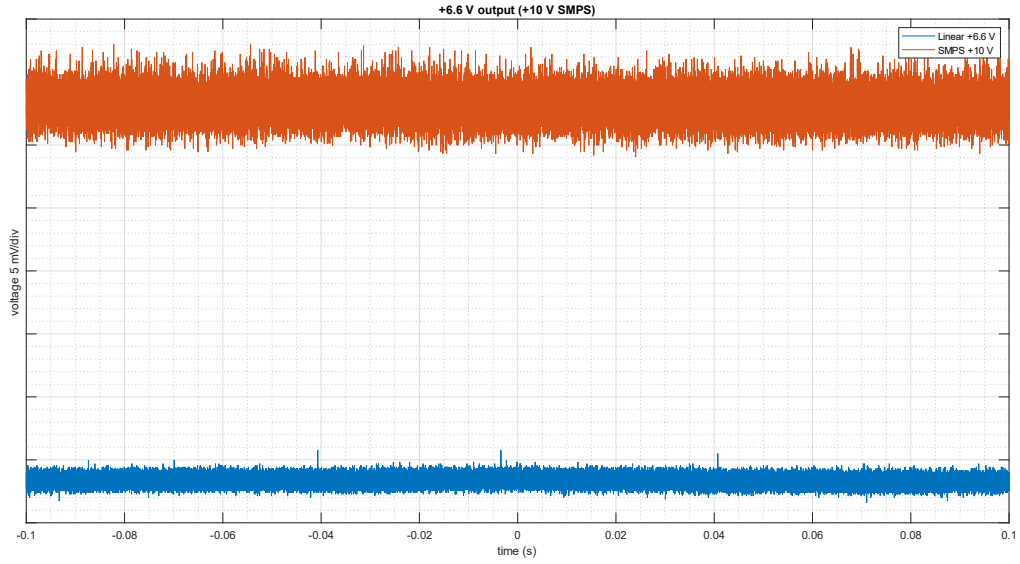

Figure A1.4. +6.6 V (+10 V SMPS) comparison in time domain

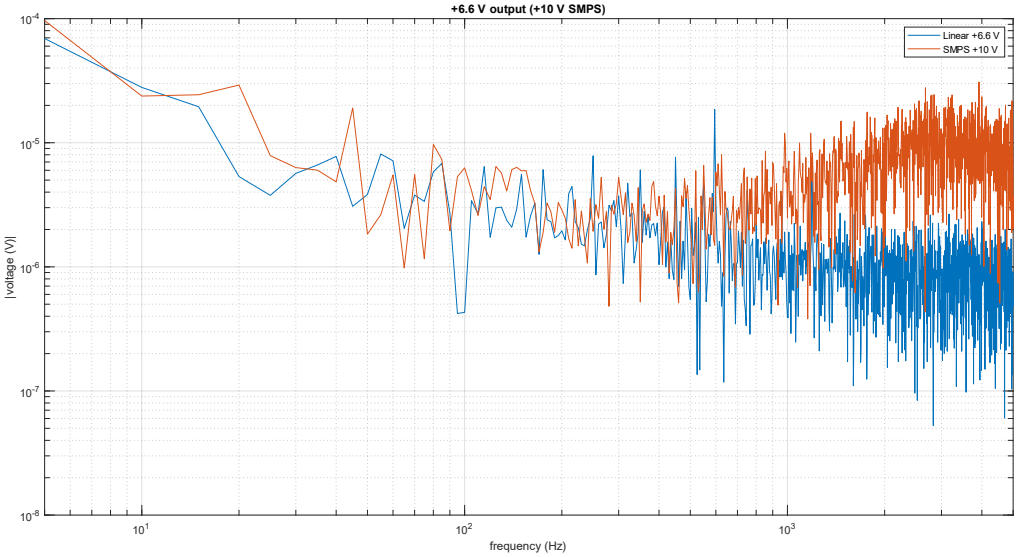

Figure A1.5. +6.6 V (+10 V SMPS) comparison in frequency domain, MEG band

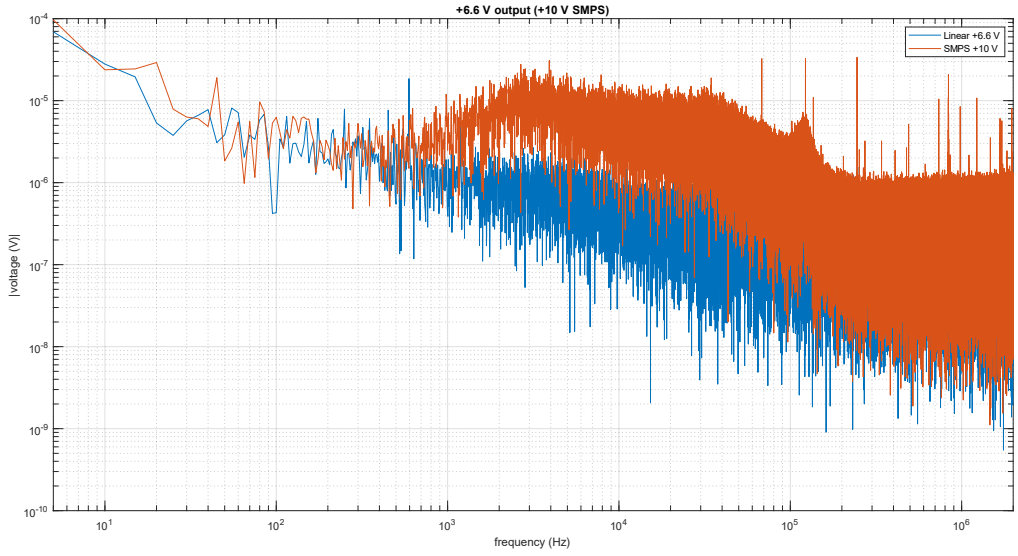

Figure A1.6. +6.6 V (+10 V SMPS) comparison in frequency domain, medium band

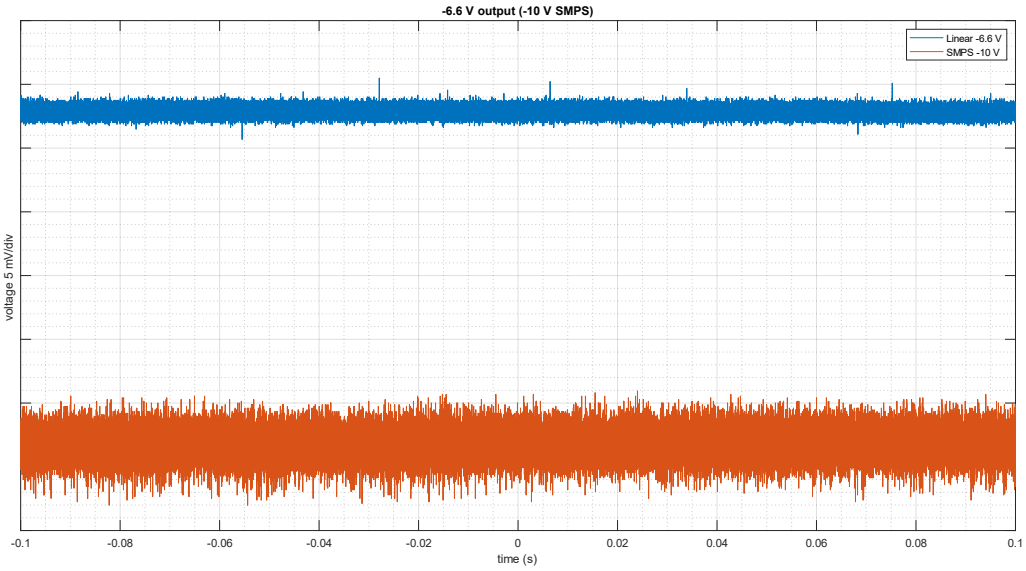

Figure A1.7. -6.6 V (-10 V SMPS) comparison in time domain

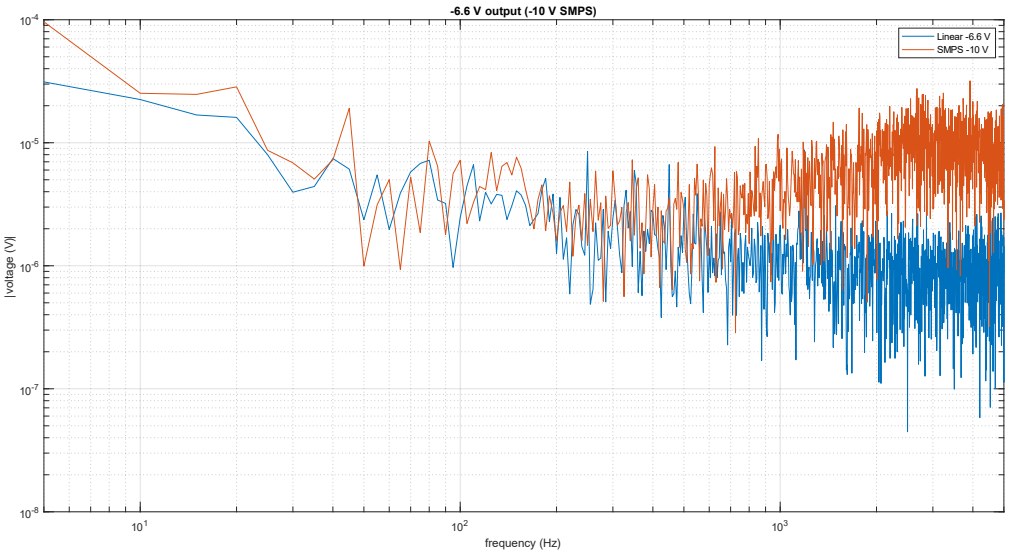

Figure A1.8. -6.6 V (-10 V SMPS) comparison in frequency domain, MEG band

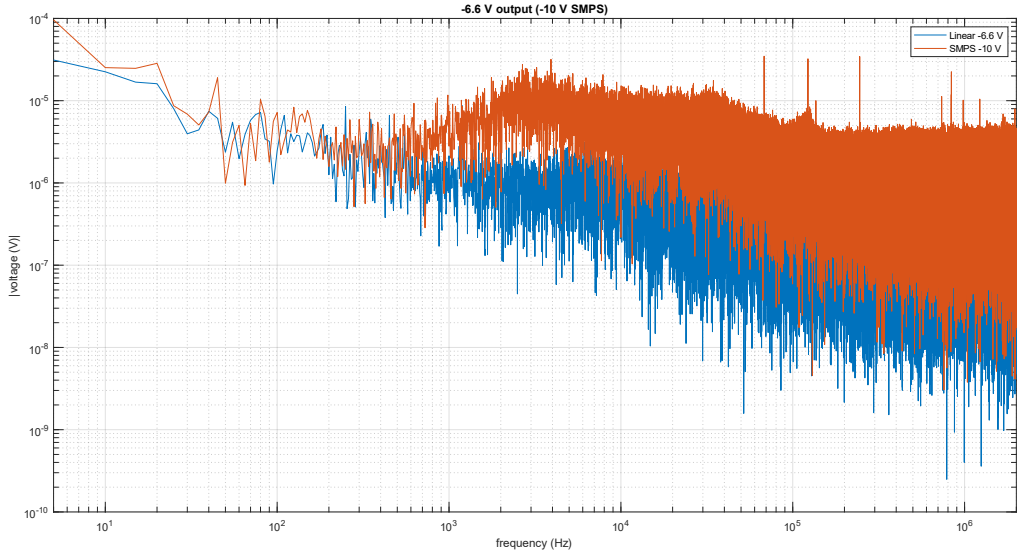

Figure A1.9. -6.6 V (-10 V SMPS) comparison in frequency domain, medium band

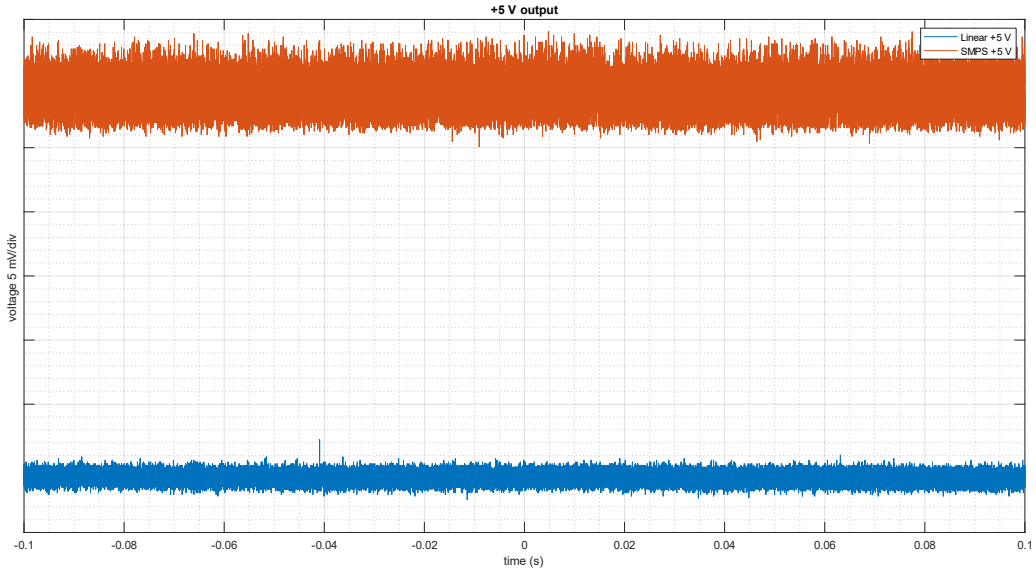

Figure A1.10. +5 V comparison in time domain

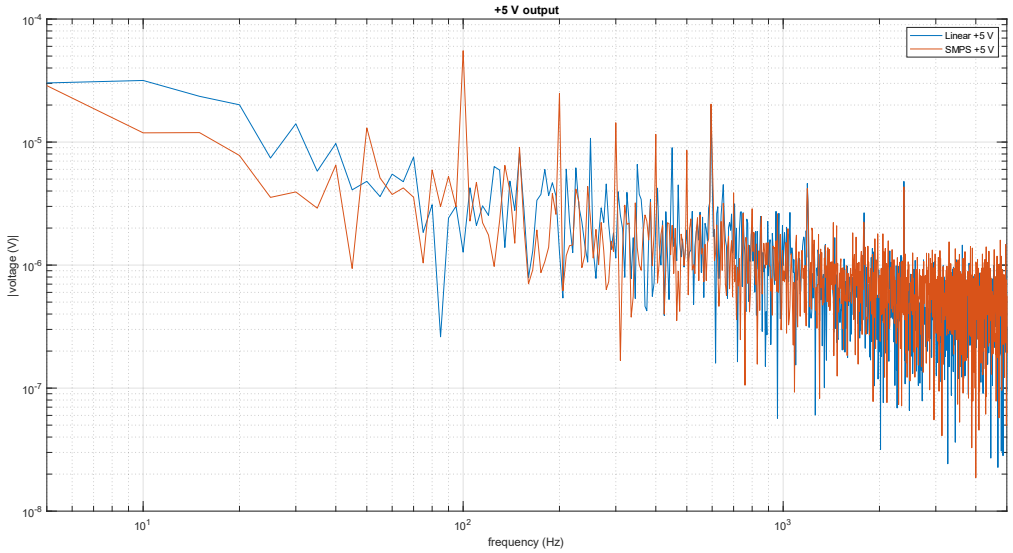

Figure A1.11. +5 V comparison in frequency domain, MEG band

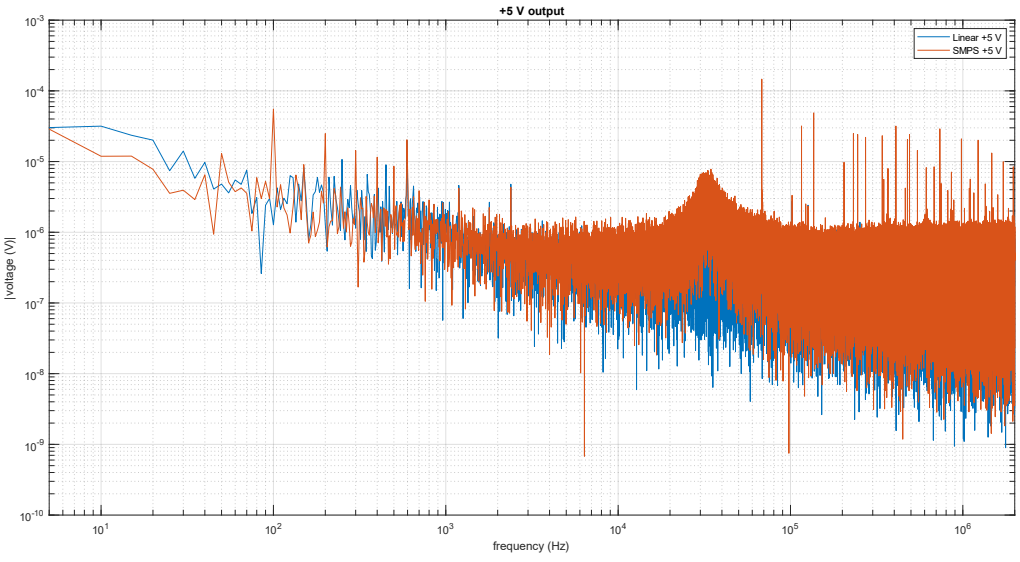

Figure A1.12. +5 V comparison in frequency domain, medium band

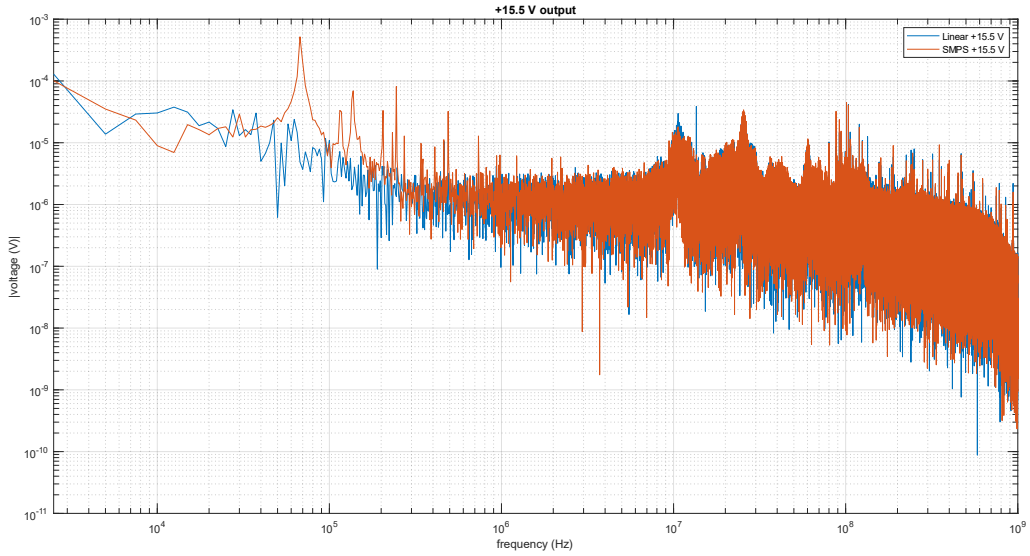

Figure A1.13. +15.5V comparison with active load, high frequency

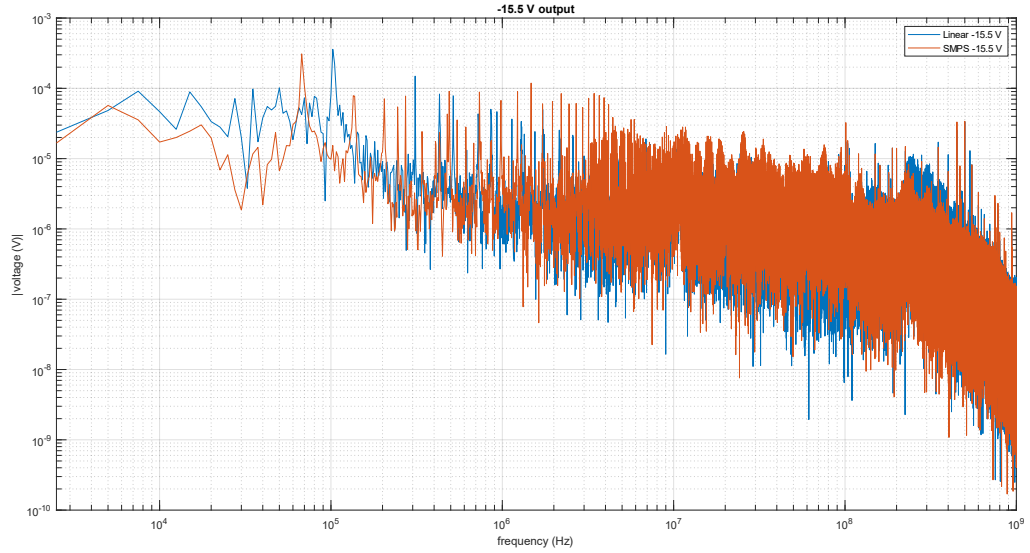

Figure A1.14. -15.5V comparison with active load, high frequency

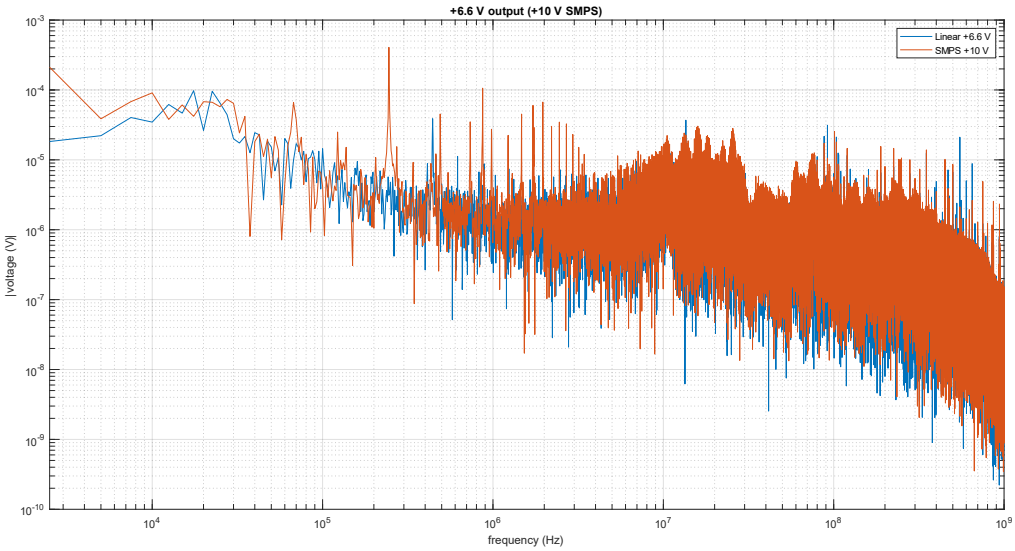

Figure A1.15. +6.6 V (+10 V SMPS) comparison with active load, high frequency

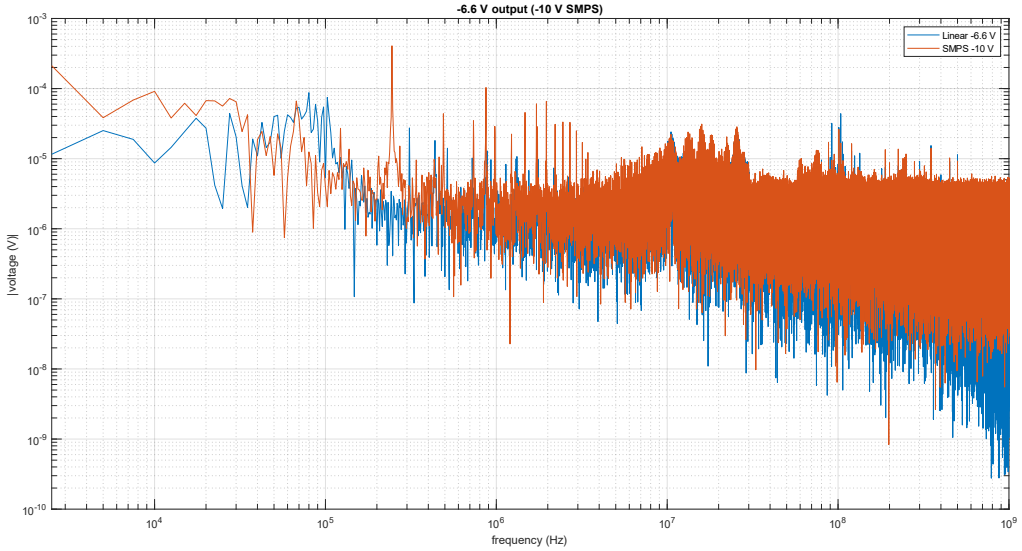

Figure A1.16. -6.6 V (-10 V SMPS) comparison with active load, high frequency

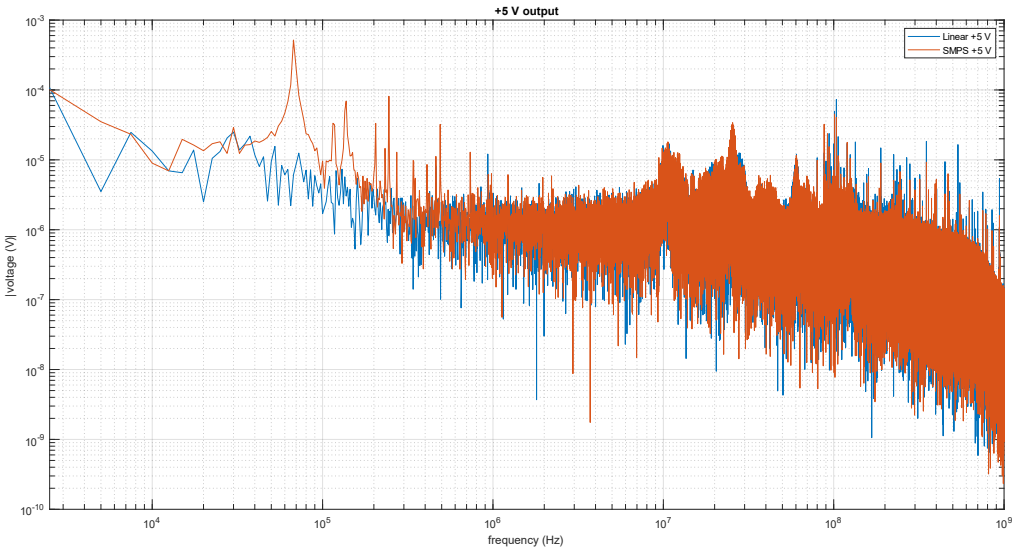

Figure A1.17. +5 V comparison with active load, high frequency

Appendix 2. Noise evaluation tool graphs

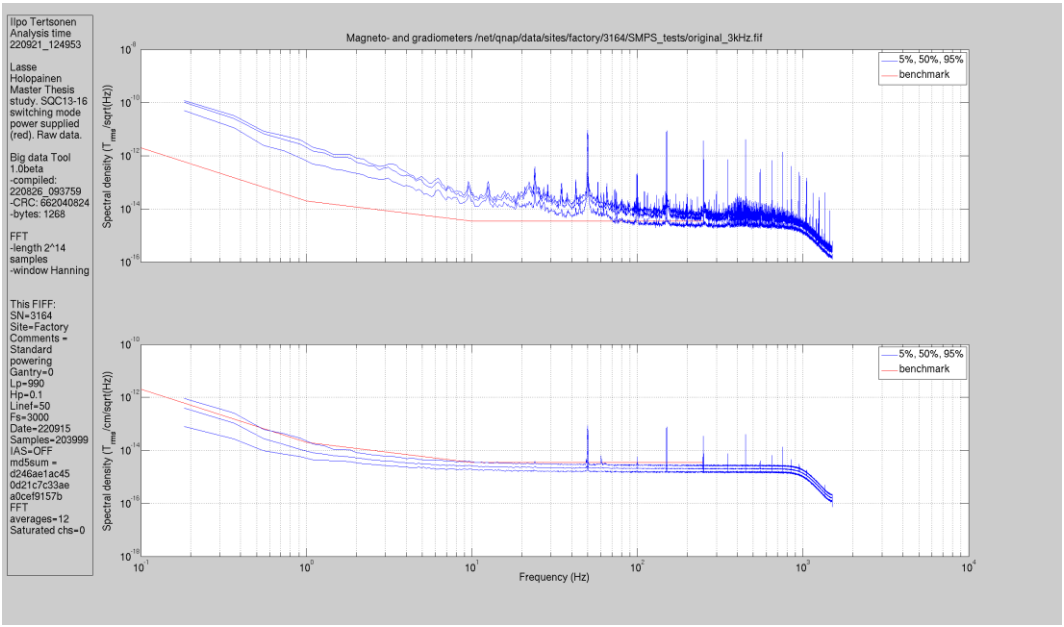

Figure A2.1. Noise spectrum: Original PSU, 3 kHz sampling frequency

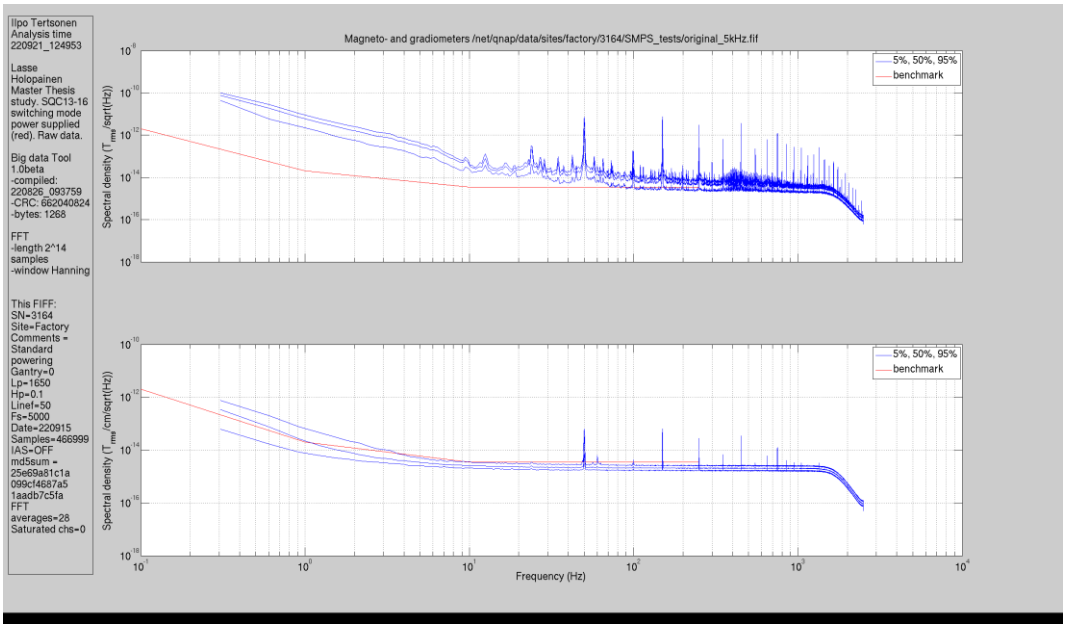

Figure A2.2. Noise spectrum: Original PSU, 5 kHz sampling frequency

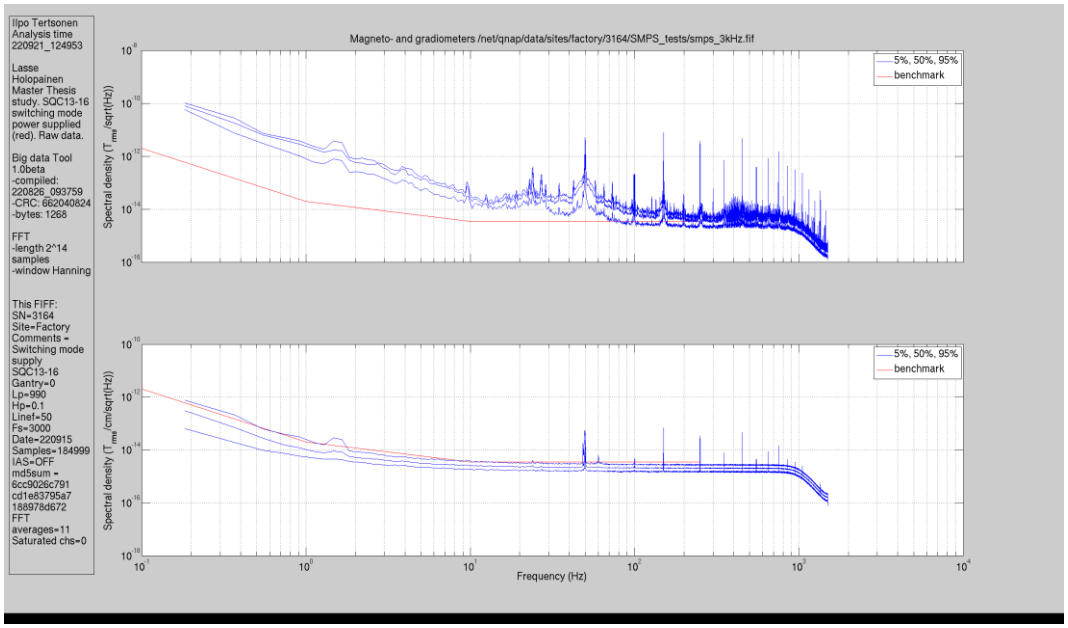

Figure A2.3. Noise spectrum: Prototype PSU, 3 kHz sampling frequency

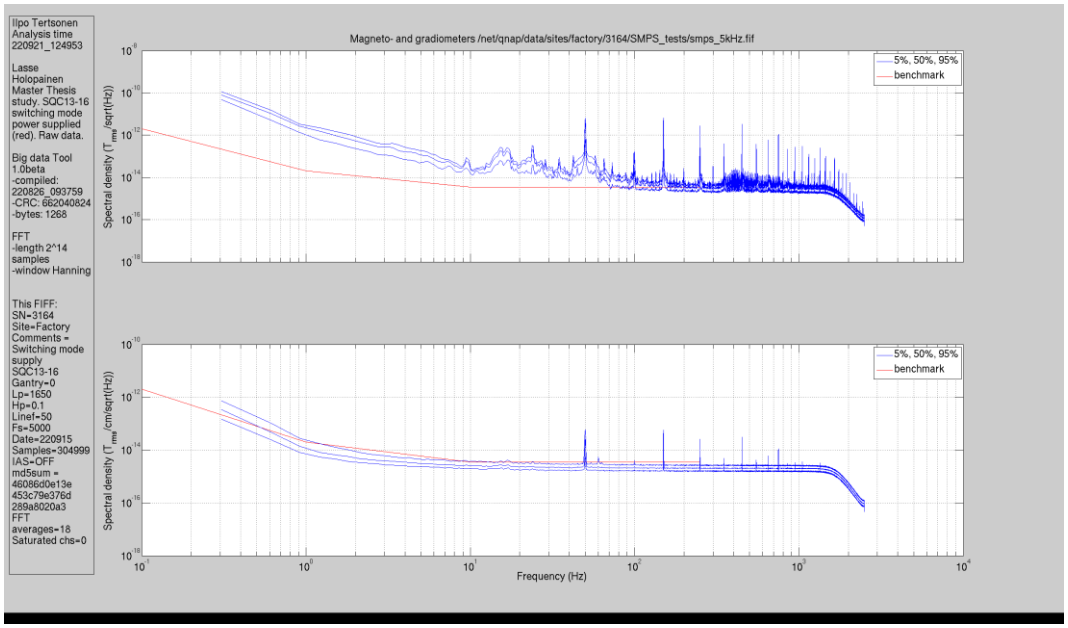

Figure A2.4. Noise spectrum: Prototype PSU, 5 kHz sampling frequency

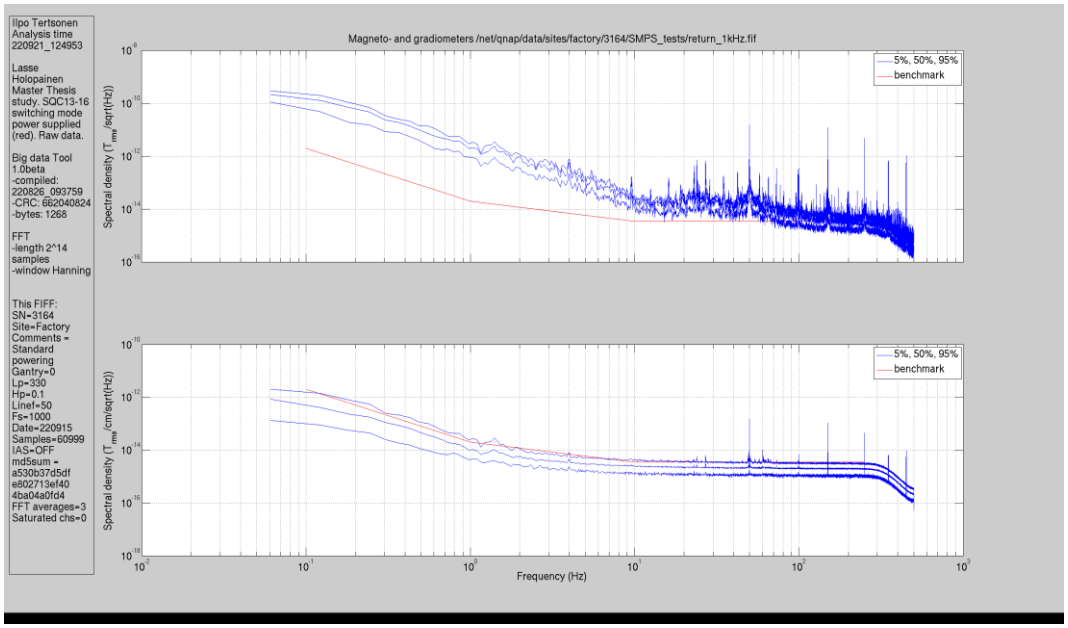

Figure A2.5. Noise spectrum: Original PSU returned, 1 kHz sampling frequency

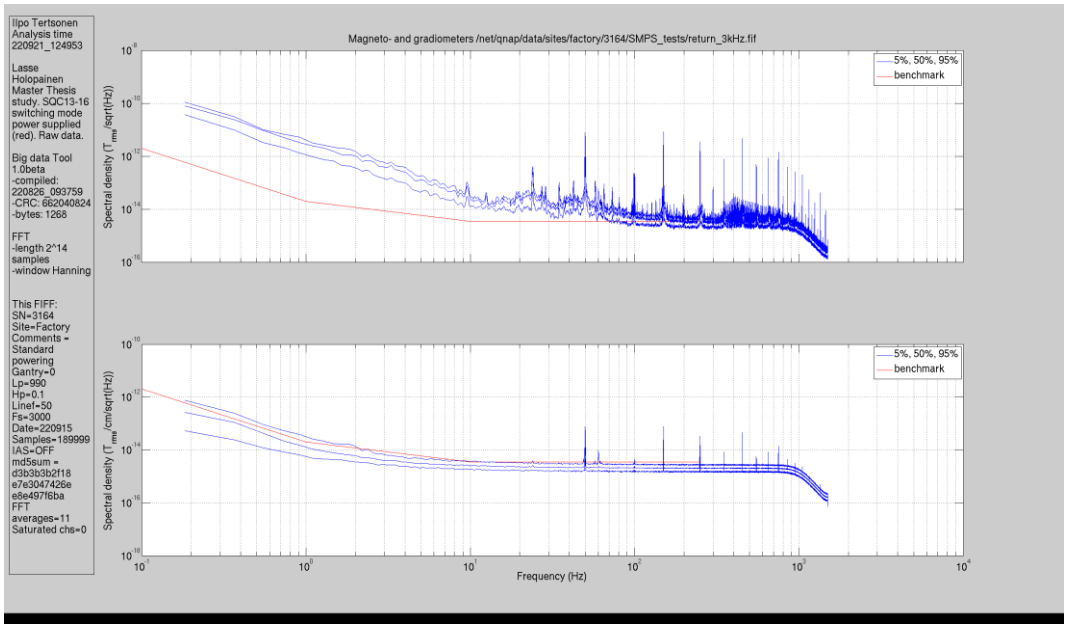

Figure A2.6. Noise spectrum: Original PSU returned, 3 kHz sampling frequency

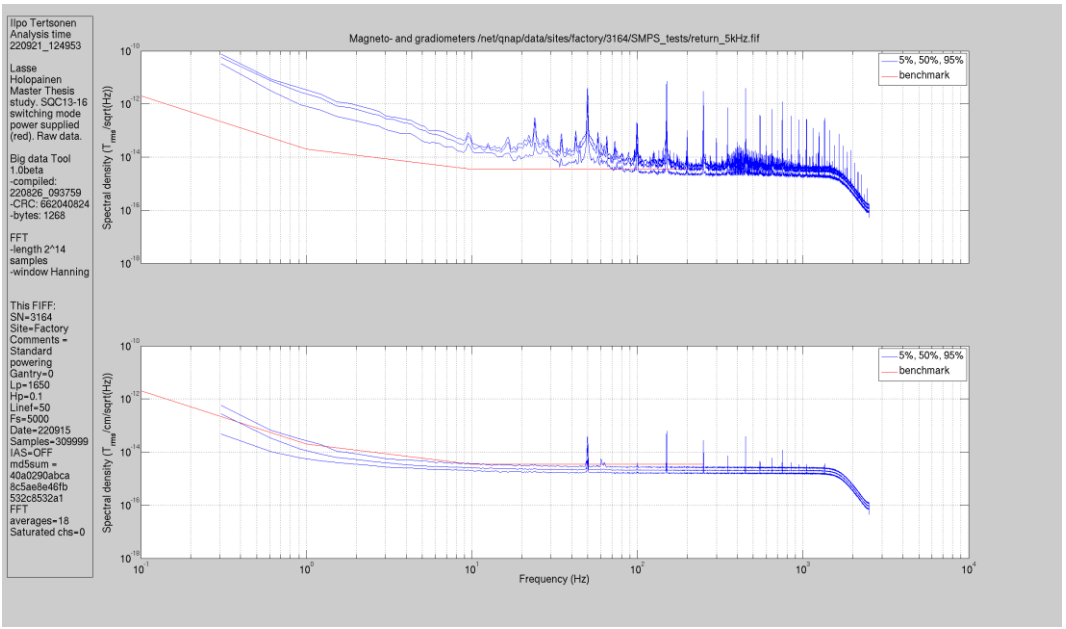

Figure A2.7. Noise spectrum: Original PSU returned, 5 kHz sampling frequency

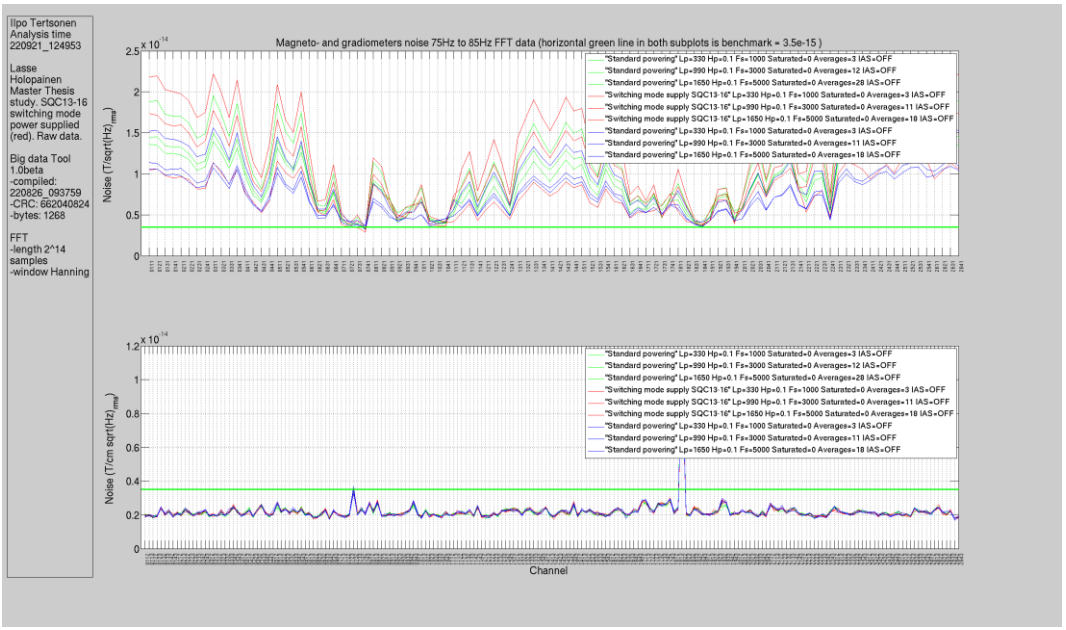

Figure A2.8. Noise FFT data, 75 to 85 Hz band

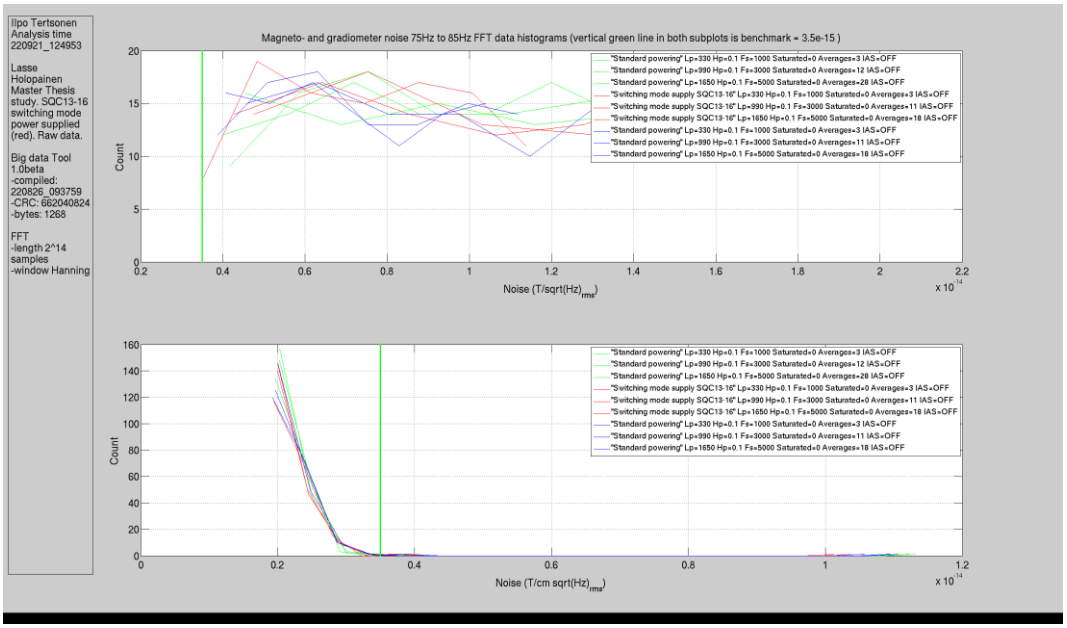

Figure A2.9. FFT data histograms, 75 Hz to 85 Hz band

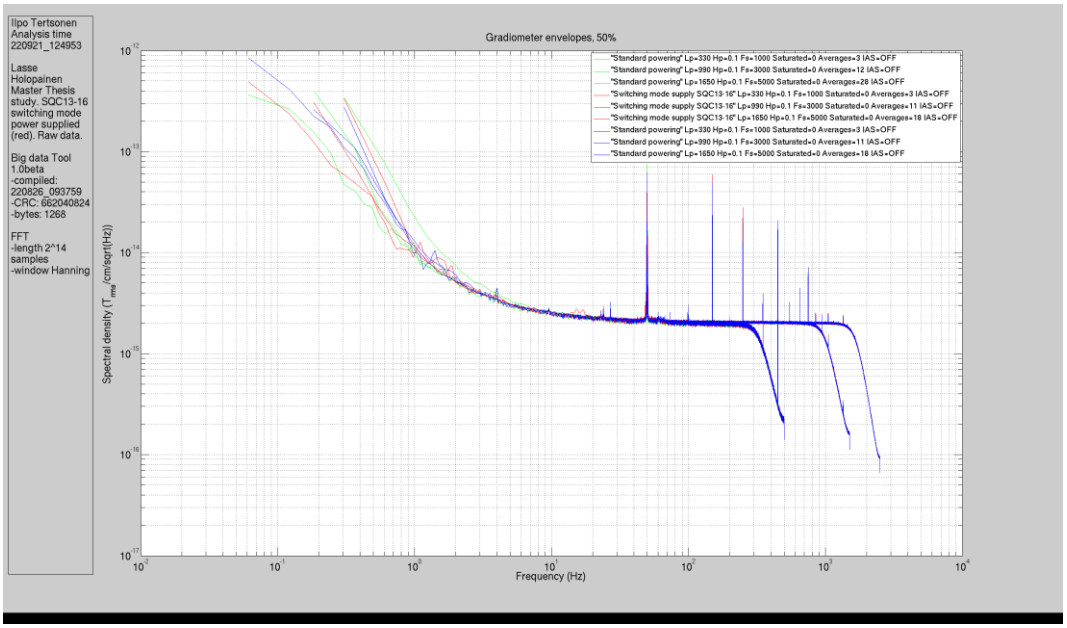

Figure A2.10. Spectral density gradiometers, 50 % envelope

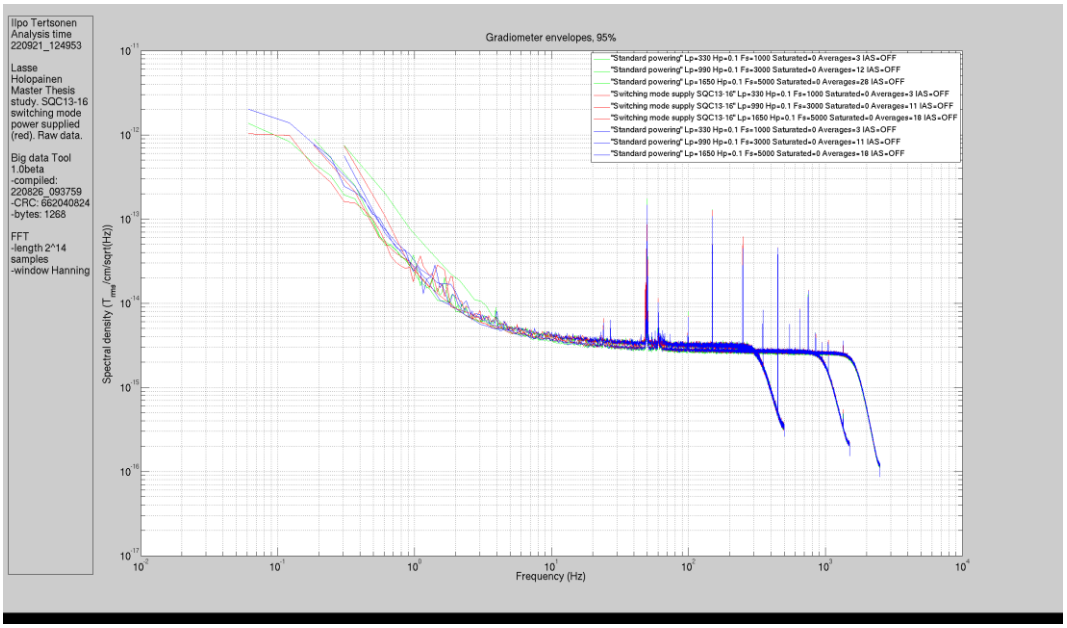

Figure A2.11. Spectral density gradiometers, 95 % envelope

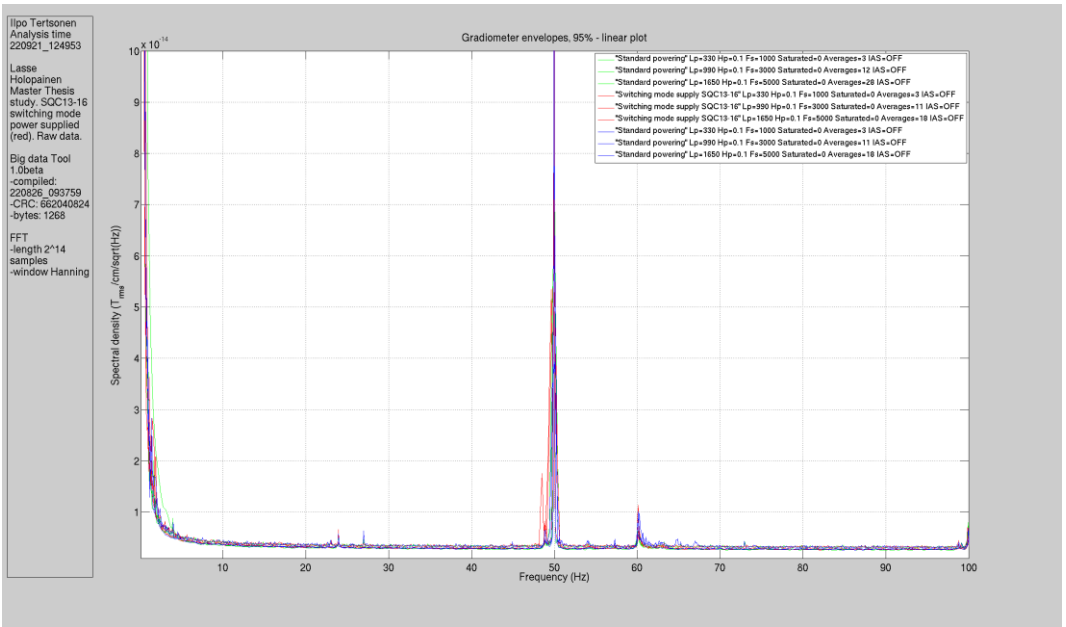

Figure A2.12. Spectral density gradiometers, linear, 95 % envelope

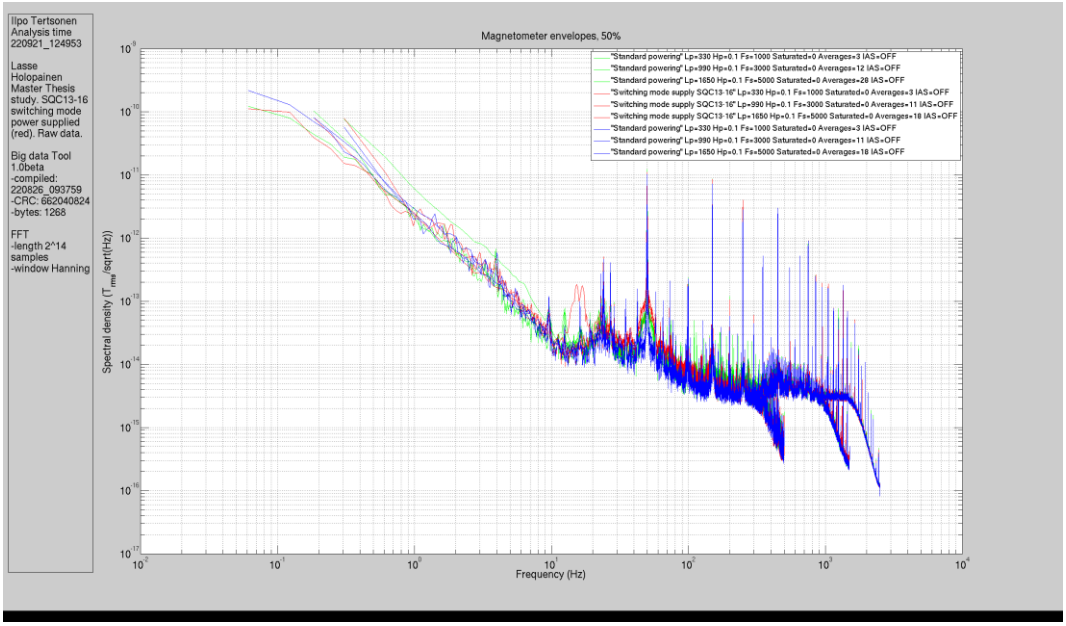

Figure A2.13. Spectral density magnetometers, 50 % envelope

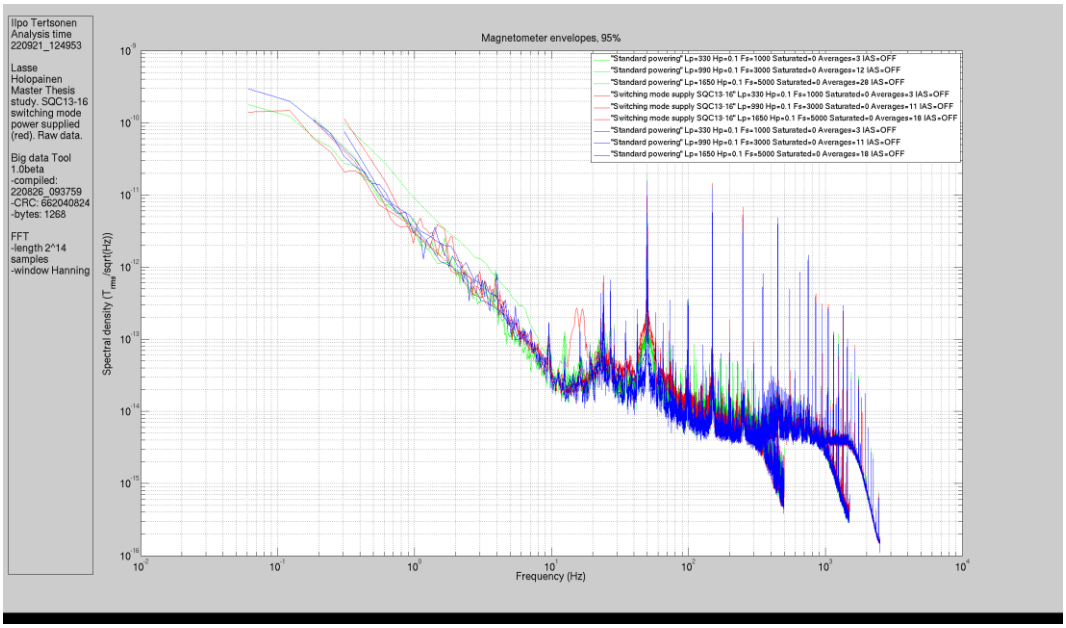

Figure A2.14. Spectral density magnetometers, 95 % envelope